Structure and stratigraphy of the Sherbrook Supersequence: 3-D seismic analysis of growth faults in the Outer Otway Basin

Thesis submitted in accordance with the requirements of the University of Adelaide for an Honours Degree in Geology & Geophysics

James William Brown

November 2019

THE UNIVERSITY of ADELAIDE

ABSTRACT

Prominent growth faulting and sediment bypass influenced the thickness of Sherbrook Supersequence sediments south of the Mussel Fault Zone in the Voluta Trough. This study quantifies the geometry and kinematics of faults and sediment dispersal in the deep-water province of the Otway Basin, offshore Victoria. A 3D seismic reflection survey was used to investigate the geometries and origin of complex linked growth fault arrays present within the Upper Cretaceous Sherbrook Supersequence in the Voluta Trough area. Five horizons and 46 faults were mapped within the confines of the OS2-3D seismic reflection survey which encompasses a 773 km² area along the present-day shelf edge in the central Otway Basin, Victoria. The resulting geological framework consists of two NW striking listric hard-linked fault arrays, as well as two NNE striking fault arrays that are crosscut by the identified NW striking fault arrays. Isopach maps of four Upper Cretaceous stratal units indicate growth of all studied faults has controlled distribution of sediments temporally throughout the study area since the Turonian or earlier. Episodes of growth faulting created scoop shaped hanging-wall depocentres and caused SW-SE basinward thickening of stratal units. Isolated hanging-wall depocentres coalesced to form large combined depocentres in subsequent strata. Growth faults overlying basement faults underwent multiple separate phases of displacement and may have been activated preferentially. Cumulative displacement of major NW-SE striking fault arrays increases SE along strike, where growth strata reach thicknesses >1500 m. Lateral throw variations along strike of fault arrays imply fault arrays once consisted of individual faults that grew independently prior to linkage. Throw variations along depth of faults reveals up to 722 m of throw present within Turonian-Santonian and age strata, and suggests faults nucleated in response to an Upper Cretaceous phase of rifting proposed by previous studies of the Otway Basin. Differential compaction of sediment above basement related topography may be an important factor influencing fault distribution within the study area.

KEYWORDS

Otway Basin, Nelson Sub-basin, 3D Seismic, Sherbrook Supersequence, Growth Faults.

TABLE OF CONTENTS

LIST OF FIGURES AND TABLES

of coherency attribute at a depth of 3000m. Survey outline (OS02-3D) shown in green dashed line. Fault array 1 = F1-F4, Fault array 2 = F4 -F8, Fault array 3 = F9-F13, Fault array 4 = F14-F20. Faults coloured for identification purposes.

Figure 7. Illustration of fault terminology. (a) Definition of fault throw, displayed on an idealised fault plane, where throw occupies a finite strain envelope that reduces to zero at tips. (b) A growth fault breaching the free surface and influencing sediment dispersal. (c) Throw profiles for faults along strike. A fault used in the study is compared to an ideal fault displacement profile. (e) Growth faulting and stratal thickness. The thickness maps of Figure 10 are equal to the difference in depth between horizons. Expansion indices are calculated by dividing the hanging-wall thickness by the footwall thickness.

Figure 8: Depth structure maps of key horizons in the study area. (a) H5; (b) H4; (c) H3; (d) H2; (e) H1. Hotter colours indicate increasing depth. See Figure 3a for horizons relative to seismic and stratigraphic framework. Contour interval for all maps = 50m.

Figure 9. T-x plots for faults F1-4 (a), F5-8 (b) F9-13 (c), and F14-20 (d). The lower panel plots the apparent throws for these faults, that is, this is a T-x plot where throw at H2 and H5 is measured along strike of the fault array parallel to the average strike of the fault array. Individual faults in each array are coloured for identification, see Figure 6 for fault locations. The upper panel shows fault-related strain along the array, calculated as the sum of the apparent heaves divided by the pre-faulting line length across the fault.

Figure 10. Throw-depth (T-Z) plots of maximum throw with depth along dip of fault planes. (a) FA1; (b); FA2; (c) FA3; (d) FA4. Individual faults in each array are coloured for identification, see Figure 6 for comparison. Throw values are based on intersection polygons for horizons shown on seismic sections in Figure 2a. See text for discussion.

Figure 11. Isopachs of key stratal units within study area; (a) SU-4; (b) SU-3; (c) SU-2; (d) SU-1. Contour interval 20m. Hotter colours indicate areas of greater thickness. See Figure 4 for stratigraphic context of stratal units. Note the thickening of strata within hanging wall depocentres.

Figure 12. Expansion index plots for faults F1-F20. Expansion index is the calculated as the ratio of thickness of a hanging-wall layer compared to the same layer in the footwall (Figure 7d). EI calculated using EI units and horizons shown in Figure 3.

Figure 13. A map of southern Australian rifting and zones of normal-oblique rifting, transitional rifting, and transform rifting. The adjacent Bight Basin is shown to the west, shaded pink. The Otway Basin is shown shaded green, and the Sorell Basin is shown in purple to the east.

Figure 14. Schematic of the fault models, after Childs et al., 2019. (a) The propagating fault model, where individual faults at T1 begin to link at T2, and finally coalesce at T3. A perspective view of this process is shown at (d). The constant-length model of faulting (c), whereby strike lengths are established early and subsequent fault growth is

predominantly by throw accrual. A perspective view of the coherent fault model is shown at (e).

Figure 15. Facies maps for the Otway Basin, during deposition of the Timboon Formation (a), Paaratte Formation (b), Nullawarre Formation (e), and Flaxman Formation (d). Key legend shown top right. Direction of sediment transport indicated by yellow arrow.

Table 1: Seismic Character of horizons mapped for EU and IU analysis. Ages and biostratigraphy from Partridge 2001.

Table 2. Fault statistics for all faults in selected arrays. Max. = Maximum Min. =

Minimum.

1. INTRODUCTION

Faults influence the architecture of sedimentary basins and play important roles in petroleum systems. Accurate geologic models and understanding of structural evolution are crucial for understanding reservoir and play elements. The advent of 3D seismic reflection data almost 45 years ago allowed significant advances in understanding of fault system geometries and kinematics (Cartwright & Huuse, 2004; Davies et al., 2004). Fault systems can be mapped in far more detail than was possible with 2D seismic data (Freeman, Yielding, & Badley, 1990). Numerous analytical methods have been developed with the aim of understanding how faults grow and behave. Techniques used to assess fault growth, kinematics, and segmentation are well documented (Giba, Walsh, & Nicol, 2012; Jackson, Bell, Rotevatn, & Tvedt, 2017; Mansfield & Cartwright, 1996; Rotevatn, Jackson, Tvedt, Bell, & Blæken, 2019). The use of such techniques can be applied to improve understanding of tectonics and basin architecture.

Structure and stratigraphy of the deep-water Otway Basin is not as well documented as onshore and coastal areas of the basin (e.g. Lovibond, Suttill, Skinner, & Aburas, 1995; Lyon, Boult, Hillis, & Bierbrauer, 2007; Palmowski, Hill, & Hoffman, 2004; Robson, Holford, King, & Kulikowski, 2018; Ryan, Knight, & Parker, 1995). Although several studies do refer to deeper parts of the basin, they do not explore the relationship between faulting, tectonics and sediment supply (Hall & Keetley, 2009; Hazar et al., 2016; Robson, King, & Holford, 2016).

The aim of this thesis is to build an accurate faulted framework model (e.g. Krantz & Neely, 2016) and to analyse fault growth history and basin evolution in the Outer Otway

Basin. In particular, the relationship between faulting and sediment supply in the Upper Cretaceous Sherbrook Supersequence is assessed using stratal thickness maps, and the temporal evolution of faulting in the study area is constrained using established fault kinematic analysis methods. Fault orientations and geometries are considered in terms of past tectonic regimes and the influence of basement terranes on faulting activity. The aim of this study is to better understand of structure and stratigraphy within reservoir intervals to enhance our understanding of petroleum prospectivity in the Otway Basin.

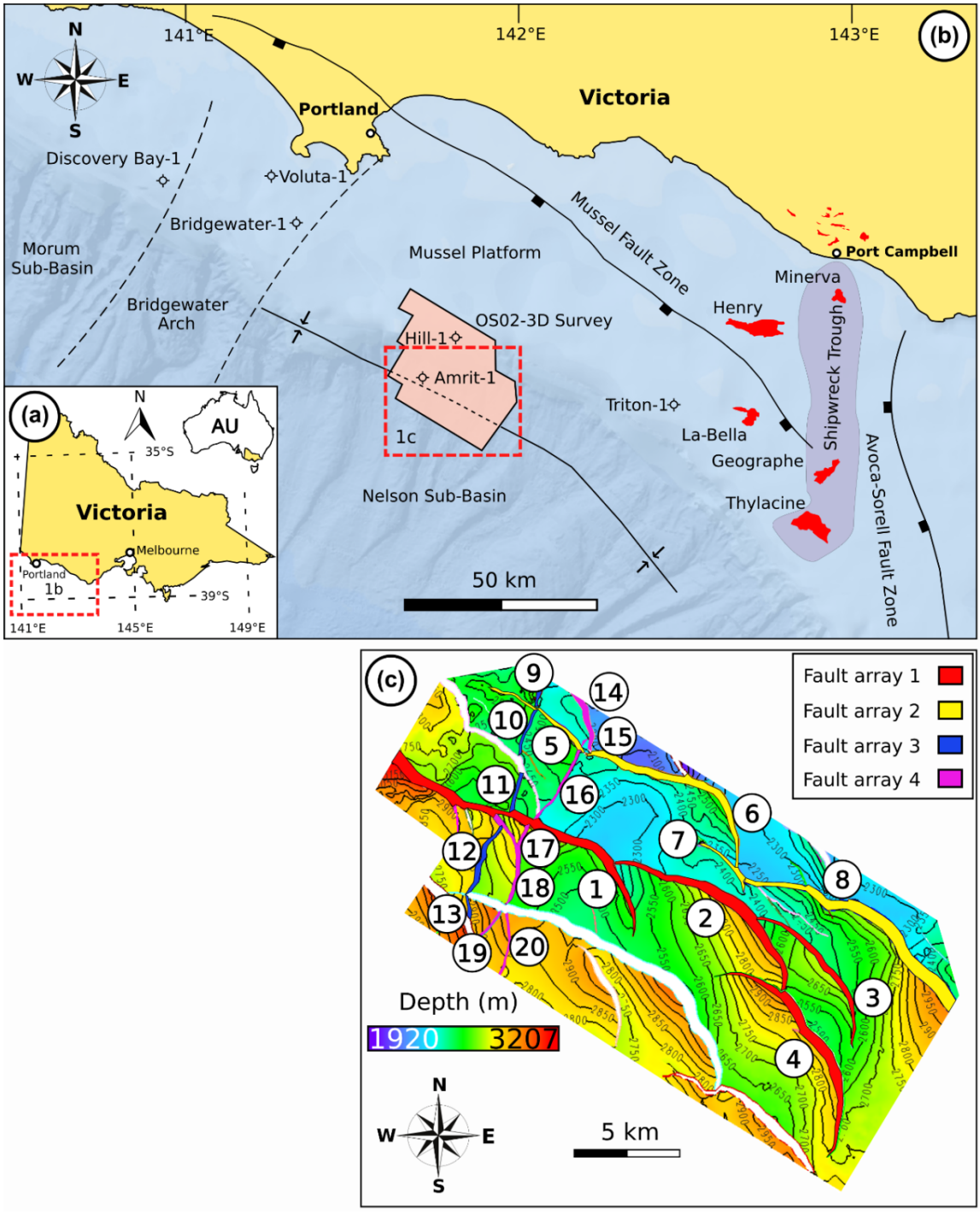

Figure 1: Location map of OS02-3D seismic reflection survey (a) relative to structural features, nearby exploration wells and gas fields. The location of the Amrit-1 well is shown, approximately 68km south of Portland Victoria, and 18km south of Bridgewater-1. The survey is positioned over the present-day shelf edge, south of the Mussel Fault Zone and Mussel Platform. The survey extends past the shelf edge and over a portion of the Nelson Sub-basin. Location inset (a) with outline of location map (b) within the state of Victoria relative to the Australian continent. Fault arrays selected for analysis are displayed in colour on a depth (metres) structure map of horizon four (c), and individual faults are numbered.

2. GEOLOGICAL SETTING

2.1 Otway Basin Tectonics

The Otway Basin is an extensional rift basin encompassing onshore and offshore parts of South Australia and Victoria, and Tasmanian waters (Figure 1). It is one of several basins that developed along Australia's southern margin during Mesozoic rifting and eventual continental separation of Australia from Antarctica. The Otway Basin developed through multi-stage rift, sag and inversion phases (Figure 2) influenced by Palaeozoic basement structures and changes in subduction activity along Gondwana's pacific margin (Hill, Finlayson, Hill, & Cooper, 1995). Rifting initiated in the Bight Basin during the Callovian and spread progressively eastward across South Australia and Victoria to open the Otway Basin during the late Jurassic-Cretaceous (Norvick & Smith, 2001). Initial rifting created the E-W trending inner Otway Basin. Upper Jurassic-Lower Cretaceous extension reactivated basement structures such as the Coorong Shear-Zone and Avoca-Sorell Fault Zone and created normal faults and half grabens with opposing NW-SE and NE-SW trends (Gibson et al., 2013).

N-S oriented faulting ceased during the Hauterivian time while faulting activity continued south of the Tartwaup Fault Zone until the end of the Barremian (Finlayson et al., 1993; Krassay, Cathro, & Ryan, 2004; Lovibond et al., 1995; Palmowski et al., 2004). Upper Cretaceous rifting shifted beneath the outer shelf and created NW-SE trending depocentres seaward of the Mussel-Tartwaup Fault Zone (Figure 1), where Palaeozoic crust thins to 25km (Briguglio, Hall, & Keetley, 2015; Finlayson, Johnstone, Owen, & Wakedyster, 1996; Hill et al., 1995; Totterdell, Hall, Hashimoto, Owen, & Bradshaw, 2014). The Mussel-Tartwaup Fault Zone consists of headwall faults involved

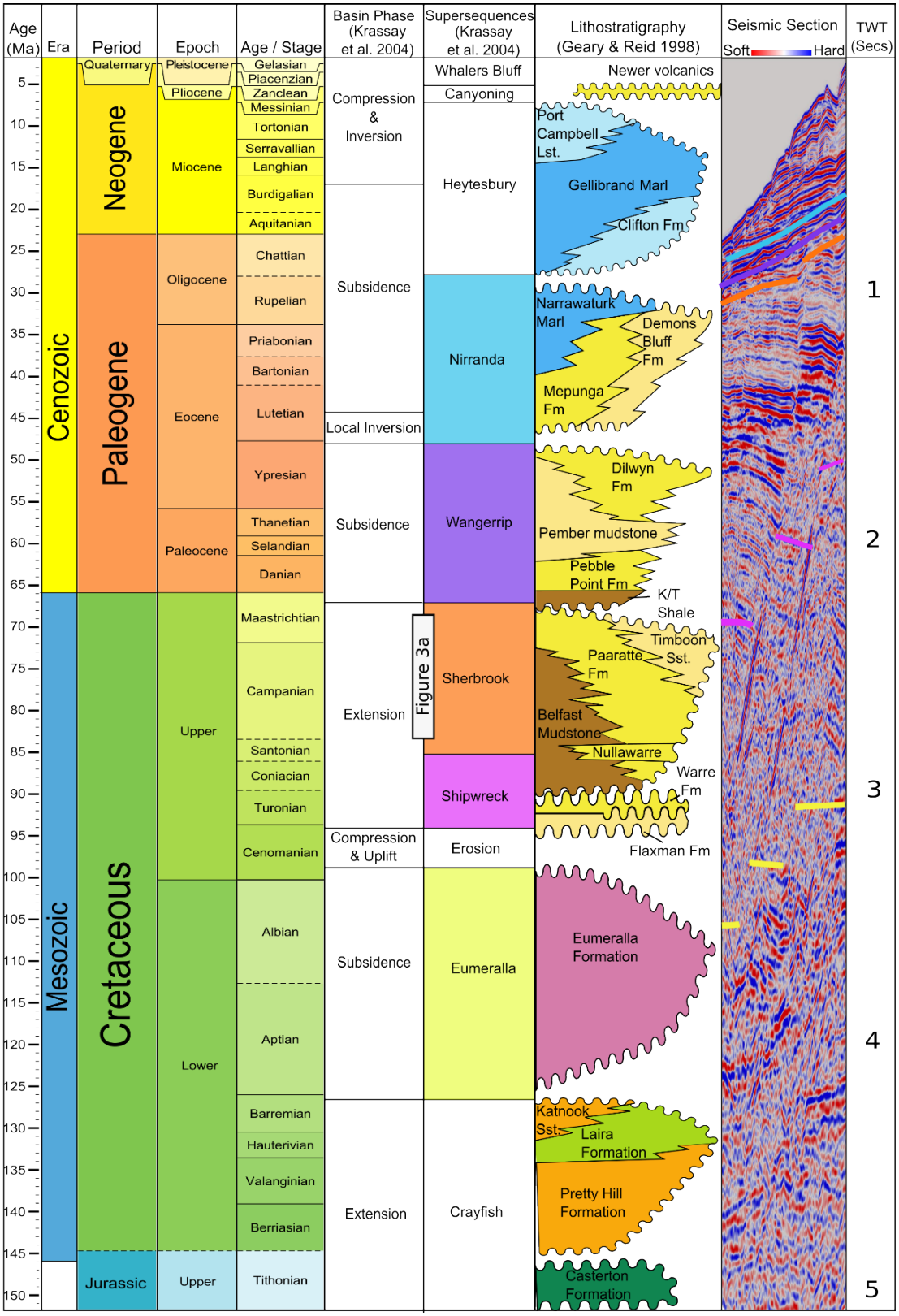

Figure 2: Otway Basin tectonostratigraphic framework modified from Krassay et al. (2004). Colour coded horizons representing tops of Supersequences from Stacey et al. (2013) are shown traced over a seismic section from seismic line DS01-108. Yellow = Eumeralla top; Magenta = Shipwreck top; Orange = Sherbrook top; Purple = Wangerrip top; Blue = Nirranda Top.

in the final separation of Australia from Antarctica (Finlayson et al., 1996). The study area is located seaward of the edge of the Mussel-Tartwaup Fault Zone at the northern edge of the Nelson Sub-basin (Figure 1) where faults have complex gravity-driven geometries and exhibit behaviours linked to deep basement-involved faults (Robson et al., 2016).

2.2 Otway Basin Stratigraphy

2.2.1 Rift initiation and & post-rift subsidence

Steady onset of rifting commenced during the Tithonian and accommodated interbedded carbonaceous lacustrine shales of the Casterton Formation (Figure 2). The Casterton Formation unconformably overlies Paleozoic basement and forms the base of the sedimentary succession in the Otway Basin (Geary & Reid, 1998; Krassay et al., 2004). Extension persisted until Berriasian times when tectonic activity resulted in a phase of erosion followed by deposition of fluvial and lacustrine facies of the Crayfish Subgroup (Krassay et al., 2004). The Crayfish Subgroup (Figure 2) consists of three units deposited during Berriasian-Barremian rifting; the Pretty Hill Formation (base unit), followed by the Laira Formation and the overlying Katnook Sandstone (Geary & Reid, 1998). A period of Aptian-Albian tectonic quiescence and thermal subsidence caused a shift in facies to thick volcaniclastic rich mudstones of the Eumeralla Formation. The Eumeralla Formation (Figure 2) is present basin-wide where depositional environments ranged from fluvial to coal swamp and lacustrine (Geary and Reid 1998). A regional unconformity caused by Cenomanian uplift and erosion separates the Lower Cretaceous Eumeralla Formation from the overlying Upper Cretaceous Sherbrook Supersequence (Krassay et al., 2004).

2.2.2 Upper Cretaceous rifting

The Sherbrook Group (Geary & Reid, 1998) consists of the older Shipwreck Supersequence (Cenomanian-Santonian age) and the Santonian-Maastrichtian aged upper Sherbrook Supersequence (Krassay et al., 2004). The basal unit of the Shipwreck Supersequence (Figure 2) consists of Turonian sands, silts and shales equivalent to the Waarre Formation. The overlying Flaxman Formation equivalent package is of Coniacian-early Santonian age. Subsequent marine transgression during the late Santonian resulted in deposition of the Belfast Mudstone (Krassay et al. 2004). The closing of an accommodation cycle marks the transition from the Shipwreck Supersequence to the Sherbrook Supersequence (Krassay et al., 2004). The upper Sherbrook Supersequence (Figure 2; Figure 3) consists of three units, the Belfast Mudstone (base), the Paaratte Formation, and the overlying Timboon Sandstone (Krassay et al., 2004).

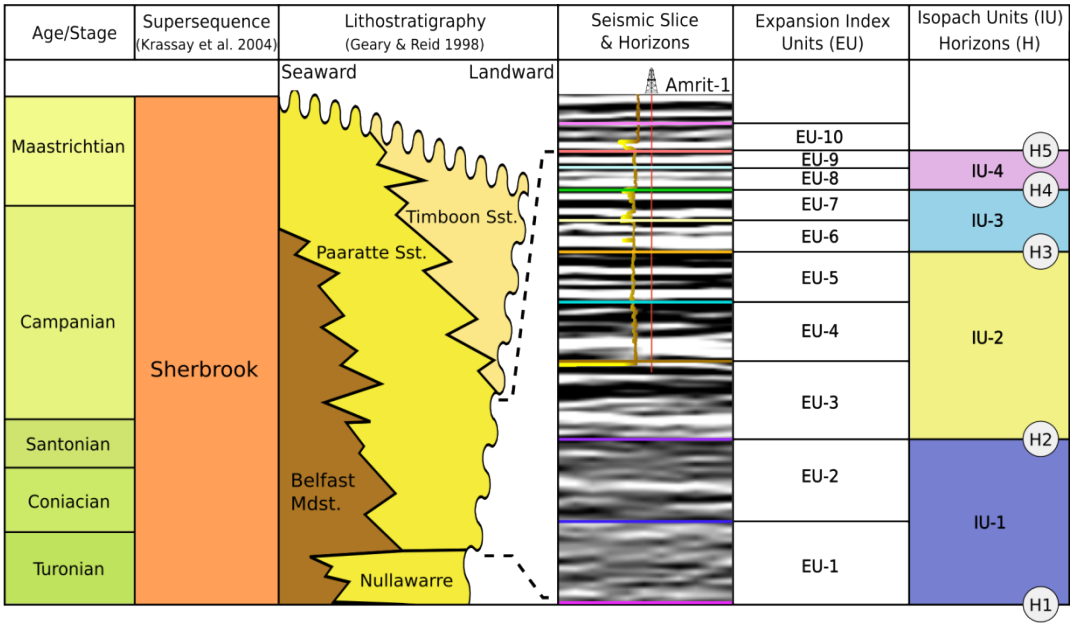

Figure 3. Stratigraphic column of the Sherbrook Supersequence. Lithostratigraphy, key lithologies and seismic stratigraphic framework for the Late Cretaceous succession in the central Otway Basin. The stratigraphic location of depth structure maps (Fig. 8) and isopach maps (Figure 11) are indicated. Additional horizons mapped locally around faults used for EU analysis (Figure 12) are shown. EU = Expansion index units; IU = Isopach units; H = seismic horizons. The horizons shown on seismic section through Amrit-1 were mapped throughout the study area. Horizons used for EI plots (Figure 12) were mapped locally around faults.

2.2.3 Upper Cretaceous break-up and Cenozoic subsidence

A period of uplift and erosion associated with Maastrichtian separation of Australia from Antarctica was followed by an extended phase of passive margin subsidence during which the overlying Cenozoic Supersequences were deposited (Krassay et al., 2004). The Wangerrip Supersequence (Figure 2) consists of Palaeocene to mid-Eocene deltaic-shallow marine units (Krassay et al., 2004). A major unconformity associated with the final breakup of Australia from Antarctica separates the Wangerrip Supersequence from the overlying Nirranda Supersequence (Krassay et al., 2004). The Nirranda Supersequence (Figure 2) is a thin condensed section of siliciclastic and carbonate lithology. The overlying Heytesbury Supersequence (Figure 2) consists of Oligocene-Miocene progradational carbonates. The Whalers Bluff Supersequence (Figure 2) consists of Pliocene-present marls and shallow marine sandstones and overlies the Heytesbury Supersequence (Krassay et al., 2004).

3. DATA AND METHODOLOGY

3.1 Seismic reflection data

This study uses 3D seismic reflection data from the offshore Otway Basin. The survey area is bordered to the north by the Mussel Fault Zone and extends south into the Nelson Sub-basin (Figure 1). The seismic survey (OS02-3D, Figure 1) consists of 773 km² full fold 3D seismic covering portions of the VIC/P51 and VIC/P52 permit areas. The inline and crossline grid spacings are both 25m. The inlines are N-S oriented and the crosslines are E-W oriented. N-S oriented inlines are perpendicular to NW-SE strike of faults, and E-W oriented crosslines trend approximately along strike. The seismic data was converted from TWT (two-way travel time) to depth in Badleys Traptester T7 software, using an interval velocity model provided by Cooper Energy (see appendix A).

3.2 Well data

The survey area encompasses the Amrit-1 exploration well (Figure 1) drilled to depth of 2979 m RT (2979 m measured well depth from the drill rig rotary table). Amrit-1 is located approximately 68km south of the town of Portland, 50km SE of Bridgewater Bay-1 and 18km SW of Hill-1 (Figure 1). The surface location of Amrit-1 is 38° 56’ 05.20” S, 141° 44’ 07.08’’ E (GDA94). Amrit-1 is used in this study to correlate horizons interpreted within the OS02-3D survey area to regional stratigraphy (Figure 3; Figure 4). Well horizon markers were obtained from company reports and previous studies of the Otway Basin (Krassay et al. 2004, Subramanian, 2005).

3.3 Mapped Horizons

Five horizons were mapped within the Sherbrook Supersequence throughout the survey area, and six additional horizons were mapped locally around selected faults (Figure 3; Figure 4). A summary of horizon characteristics is provided in Table 1. The study area has insufficient data to constrain exact ages of horizons, since biostratigraphy and a comprehensive sequence stratigraphic framework specific to the study area is not available in public literature, and the OS02-3D contains only two wells and complex stratigraphy. Approximate ages and lithologies were obtained from company reports and previous studies of the Otway Basin (Krassay et al. 2004, Partridge 2001, Subramanian 2005).

Table 1: Seismic Character of horizons mapped for EU and IU analysis. Ages and biostratigraphy from Partridge 2001.

Horizon	Phase	Amplitude	Continuity	Lithology	Formation	Sp. Zone	Age	Ma
11	Peak	Low	Excellent	Shale	Timboon	F. longus	Maast.	(~70)
10 (H5)	Trough	High	Good	Sand	Timboon	F. longus	Maast.	(~70)
9	Peak	High	Poor	Sand	Paaratte	X. australis	Camp.	(~78)
8 (H4)	Peak	High	Poor	Sand	Paaratte	X. australis	Camp.	(~80)
7	Peak	Moderate	Poor	Sand	Paaratte	N. aceras	Camp.	(~82)
6 (H3)	Peak	High	Excellent	Shale	Paaratte	O. porifera	Sant.	(~85)
5	Peak	High	Good	Shale	Paaratte	O. porifera	Sant.	(~86)
4 (H2)	Peak	Moderate	Poor	Silt	Paaratte	N. senectus	Sant.	
3	Peak	Low	Good	Shale?	Paaratte	?	Sant.	
2	Peak	Low	Good	Shale?	Belfast	?	Sant.	
1 (H1)	Peak	Moderate	Excellent	Shale?	Belfast	?	Turo.	

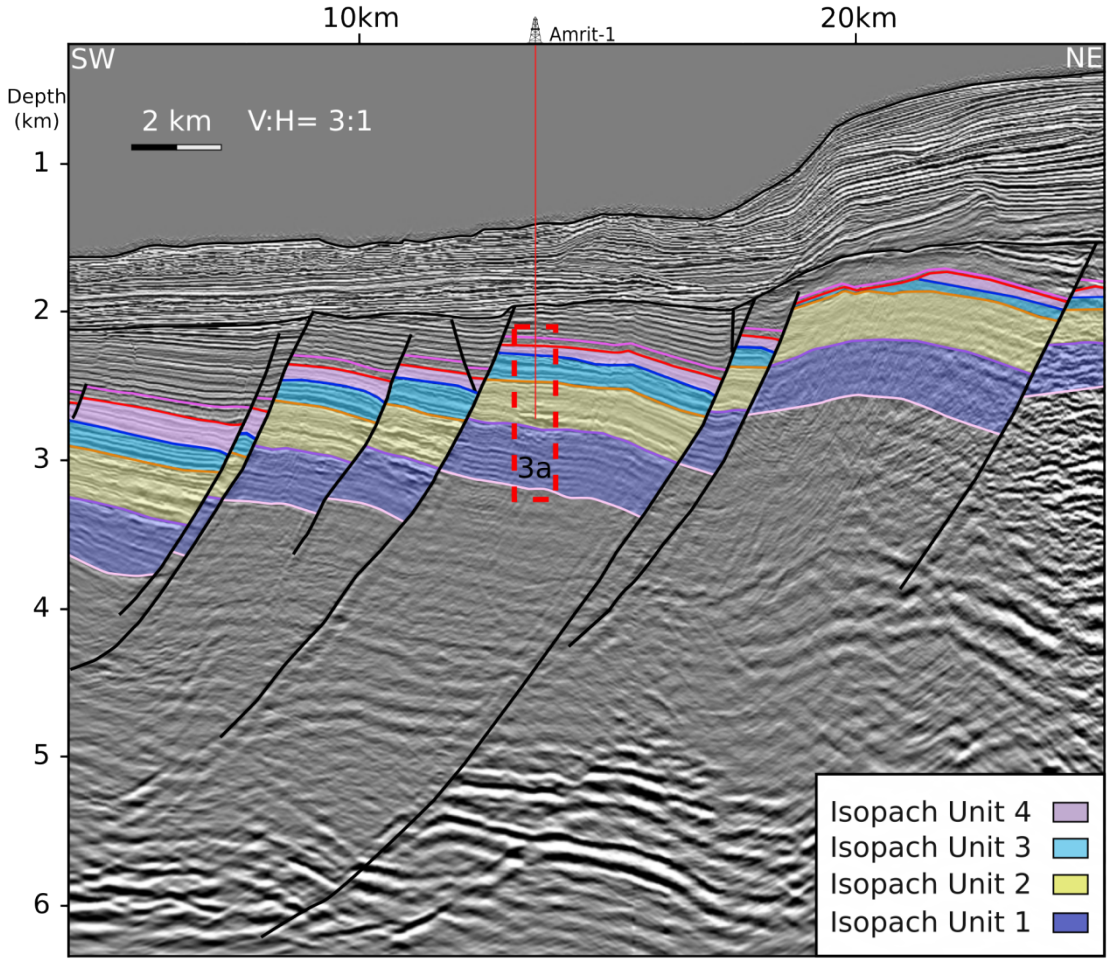

Figure 4. Down-dip (NE-SW trending) seismic cross-section shown through the OS02-3D survey area. Colour key to isopach units used for isopach analysis (Figure 3; Figure 11) pictured at bottom right. Stratigraphic location of Figure 3 on is shown in dashed red box on seismic section.

3.4 Framework Creation

A 3D framework model as described by Krantz and Neely (2016) was built using Badleys Traptester software and a standard set of workflows outlined by Yielding and Freeman (2016). The order of procedures used is summarised below. For a more detailed description of methods used, see appendix A.

3.4.1 Faults

Unassigned fault segments were traced on seismic cross sections. Fault segments are traced where offset is visible. Segments were picked on every 10th inline and crossline, resulting in an evenly spaced mesh of fault segments spaced at 250m intervals (Figure 5a). Unassigned fault segments were selected and assigned to individual fault planes with the aid of variance attribute time slices and probes used as a guide (Figure 5a). Fault plane tri-meshes were initially created using unconstrained triangulation and checked for unrealistic bumps typical of poorly picked fault segments (Figure 5b). Seismic slices of seismic amplitude were projected onto fault planes to aid precise positioning of intersecting faults. Branch lines were traced onto fault surfaces at intersections and fault surfaces re-modelled. Final fault surfaces were gridded (Figure 5c) using a grid cell dimension of 60m, approximately ¼ the distance between fault segments (Boult, Freeman, & Yielding, 2016).

3.4.2 Horizons

Horizon seed data were traced on every 20th row and column, resulting in a grid spaced at 500m intervals (Figure 5a). Horizons were first picked on arbitrary line cross sections intersecting the Amrit-1, then extended towards the edges of the survey. Horizon seed data were traced along reflectors interpreted to be a uniform time surface. Horizon seed data were made to terminate at known fault planes, seed data did not intersect fault planes. A loop-tying approach was used to check the internal consistency of horizons. A 3D auto-tracker tool within Badleys Traptester software (TT7) was used to automatically populate horizon data laterally through the seismic volume.

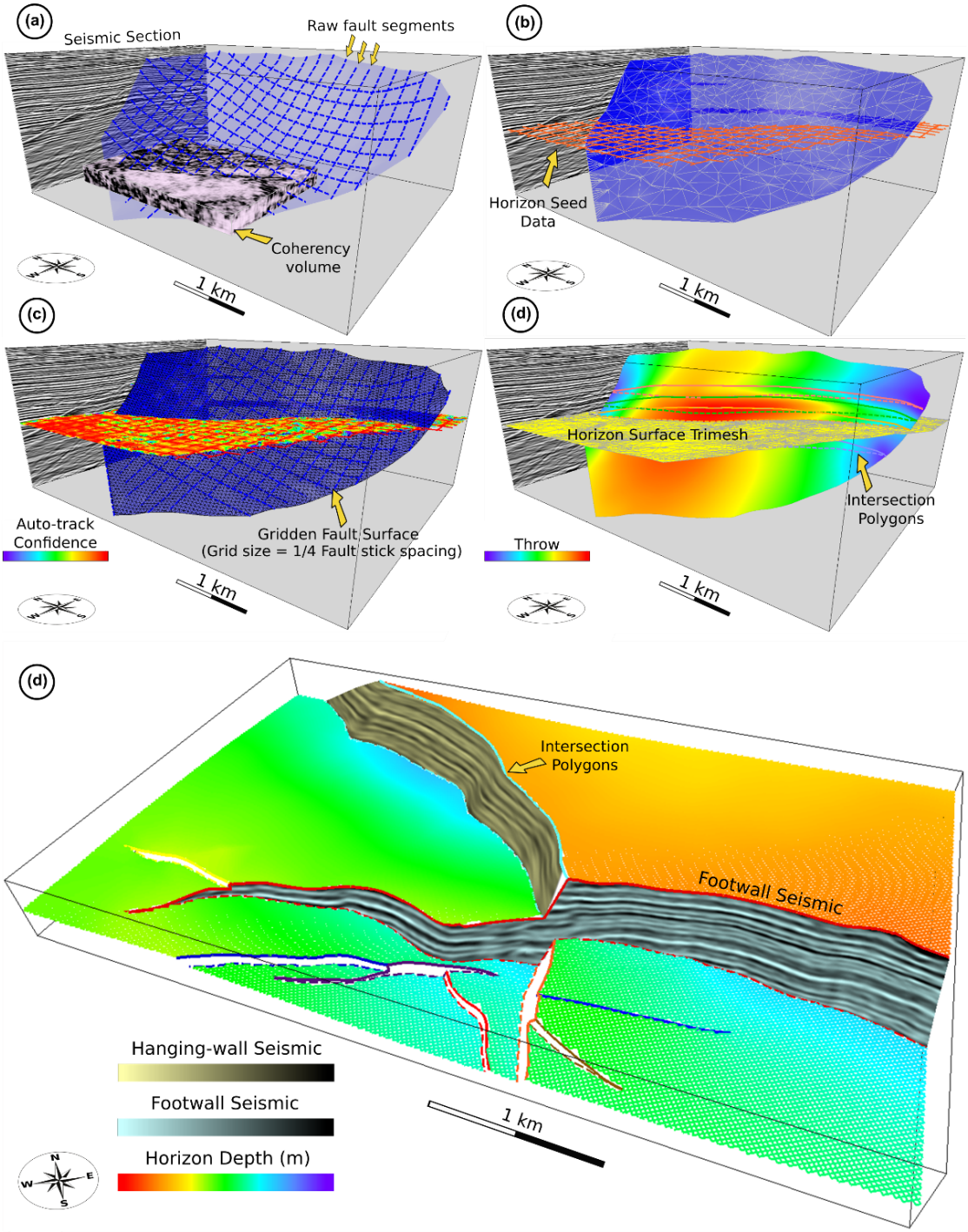

Figure 5. Four stages illustrating the procedure for interpreting seismic data and building a framework model - demonstrated with a single fault and the Paaratte K93 horizon. (a) Fault segments picked on inlines and crosslines at 250 m increments. Example of coherency attribute volume used as a guide to group fault segments shown as box. (b) A triangulated fault surface shown in blue and orange raw horizon seed data picked on inlines and crosslines at 250m grid spacings. (c) Gridded fault surface (blue) and horizon auto track data displayed as autotrack confidence. (d) Three sets of horizon intersection polygons - dashed lines represent footwalls and solid lines represent hanging walls. Fault surface coloured by fault throw attribute. Hotter colours indicate areas of larger throw values. Horizon surface tri-mesh created from autotrack horizon data displayed in yellow. (e) Complete framework model example, with seismic amplitude slice projected on to fault hanging-wall and footwall. Intersection polygons labelled.

3.4.3 Horizon-Fault Intersection Polygons:

Lines created where a horizon joins an intersecting fault, referred to in this study as intersection polygons, are sometimes called horizon cutoffs or horizon separation polygons (Yielding & Freeman, 2016). Intersection polygons are important components of an "air-tight framework" (Boult et al., 2016). Using Badleys TT7 software package, intersection polygons were traced along fault planes where horizons intersect the fault plane, and seismic slices of both hanging-wall and footwall were created 50m away from modelled fault planes and projected onto the fault surfaces as display attributes to guide editing of intersection polygons (Figure 5e). Intersection polygons were generated for five horizons (H1-H5).

3.4.4 Horizon surface creation:

Auto-track horizon data were converted to surface tri-meshes using the maximum vertices triangulation method with the maximum vertices set to 30000 (Figure 5d). The triangulation process honours both horizon raw data and intersection polygon data. Triangles were excluded from spaces between intersection polygons. Intersection polygons of all faults interpreted within the survey were used for surface creation of horizons H1-H5.

3.5 Fault Geometry

During seismic interpretation 20 of the identified fault planes were selected for analysis, hereafter referred to as F1-F20 (Figure 6). Fault planes F1-F20 were then grouped into four fault arrays based on along-strike linkage and common dip and strike orientations. Fault arrays are hereafter referred to as FA1-FA4 (Figure 1c). Geometric qualities of each fault in FA1-FA4 were generated and measured using the TT7 fault statistics and plot viewer tool. A map view of fault geometries was created for horizons H1-H5 with depth displayed in metres and gaps between fault intersection polygons. Fault qualities measured include throw (vertical component of fault displacement, see Figure 7a), maximum and minimum depth of fault tips, maximum and minimum dip values, and minimum and maximum strike values (Table 2).

3.6 Determination of fault growth

Fault displacement analysis and isopach analysis (figure 7d) are established techniques for understanding structural and kinematic evolution of rift basins (Jackson et al., 2017). Techniques used to determine the kinematics of synsedimentary faults are described below.

3.6.1 T-x plots

Throw variation along fault strike length was assessed in this study to analyse growth of individual faults and to assess lateral fault segmentation and linkage relationships within fault arrays (Huang et al., 2018; Tvedt, A., Rotevatn, A., Jackson, C., Fossen, H., & Gawthorpe, R., 2013). Throw is defined in this study as the vertical component of fault displacement (Figure 7a). Using Badleys T7 software, throw was plotted along fault

strike to create T-x plots. Throw measurements were calculated in Traptester using intersection polygons generated for H2 and H5 during the seismic interpretation process (Figure 4e).

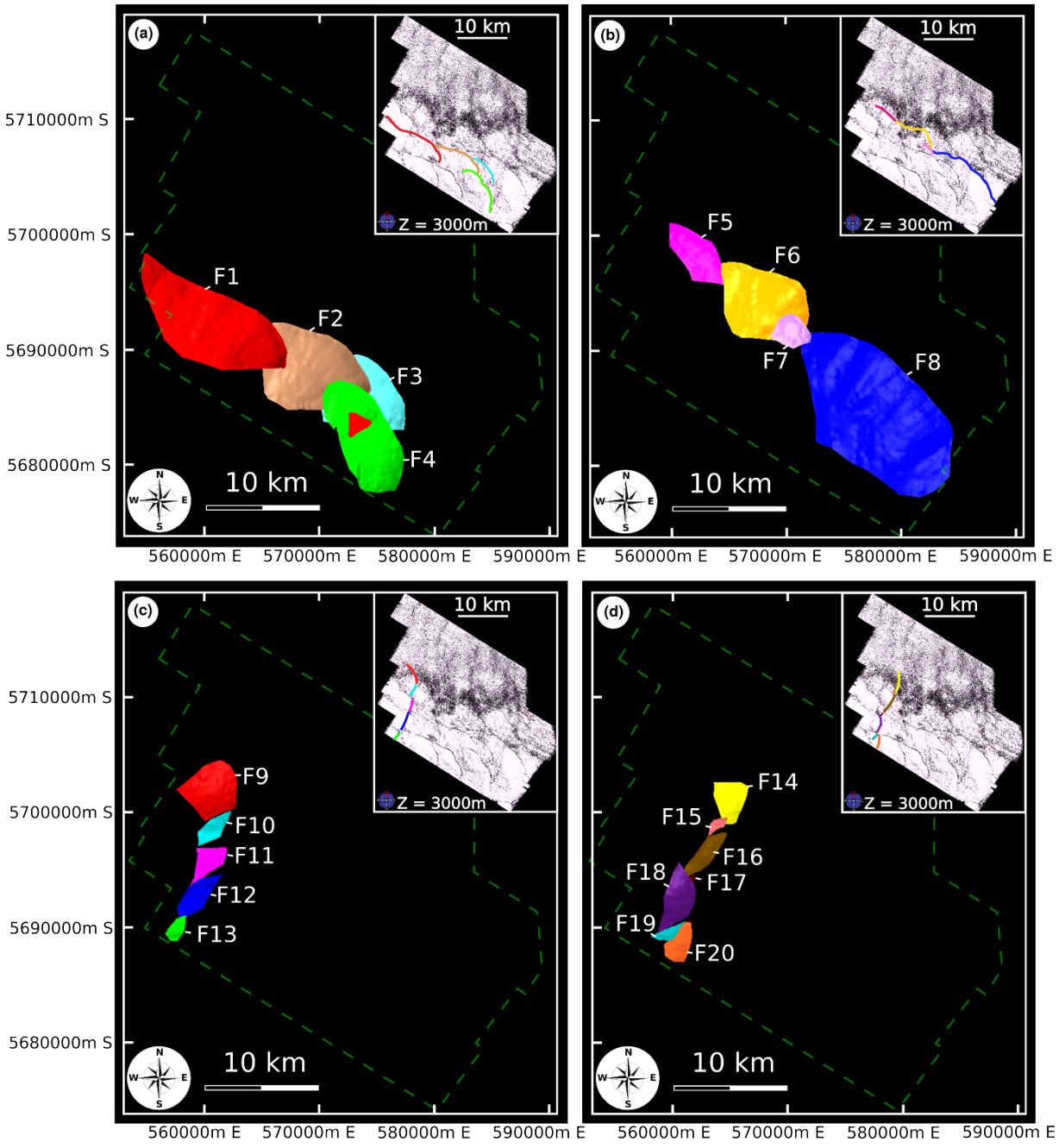

Figure 6. 3D geometry of fault arrays shown in map view. (a) Fault array 1; (b) Fault array 2; (c) Fault array 3; (d) Fault array 4. Fault locations traced on horizontal (Z slice) of coherency attribute at a depth of 3000m. Survey outline (OS02-3D) shown in green dashed line. Fault array 1 = F1-F4, Fault array 2 = F4 -F8, Fault array 3 = F9-F13, Fault array 4 = F14-F20. Faults coloured for identification purposes.

3.6.2 T-z plots

Analysis of throw and throw variation with depth was used in this study to infer depth and timing of fault nucleation and to analyse vertical segmentation and dip linkage of faults (Baudon & Cartwright, 2008; Mansfield & Cartwright, 1996; Robson et al., 2016, 2017). Using Badleys T7 software, maximum throw was plotted along fault depth (metres) to create T-z plots (Mansfield & Cartwright, 1996). Throw measurements were derived from intersection polygons generated for horizons H1-H5 during the seismic interpretation process (Figure 4e).

3.6.3 Isopach maps

Isopach maps were created to measure sediment accumulation in response to fault related accommodation and subsidence (Jackson & Rotevatn, 2013). Isopach maps are thickness maps that record areas of syn-kinematic sediment deposition and therefore record the evolution of growth faults (Jackson et al., 2017). Growth faults create scoop shaped depocentres where hanging-wall growth strata thicken (Figure 7d) at points of maximum displacement (Gawthorpe & Leeder, 2000). Isopach maps were created by using Badleys T7 software to calculate thickness of strata between horizons H1-H2, H2-H3, H3-H4 and H4-H5, all of which were generated during framework model creation (Figure 4a-e).

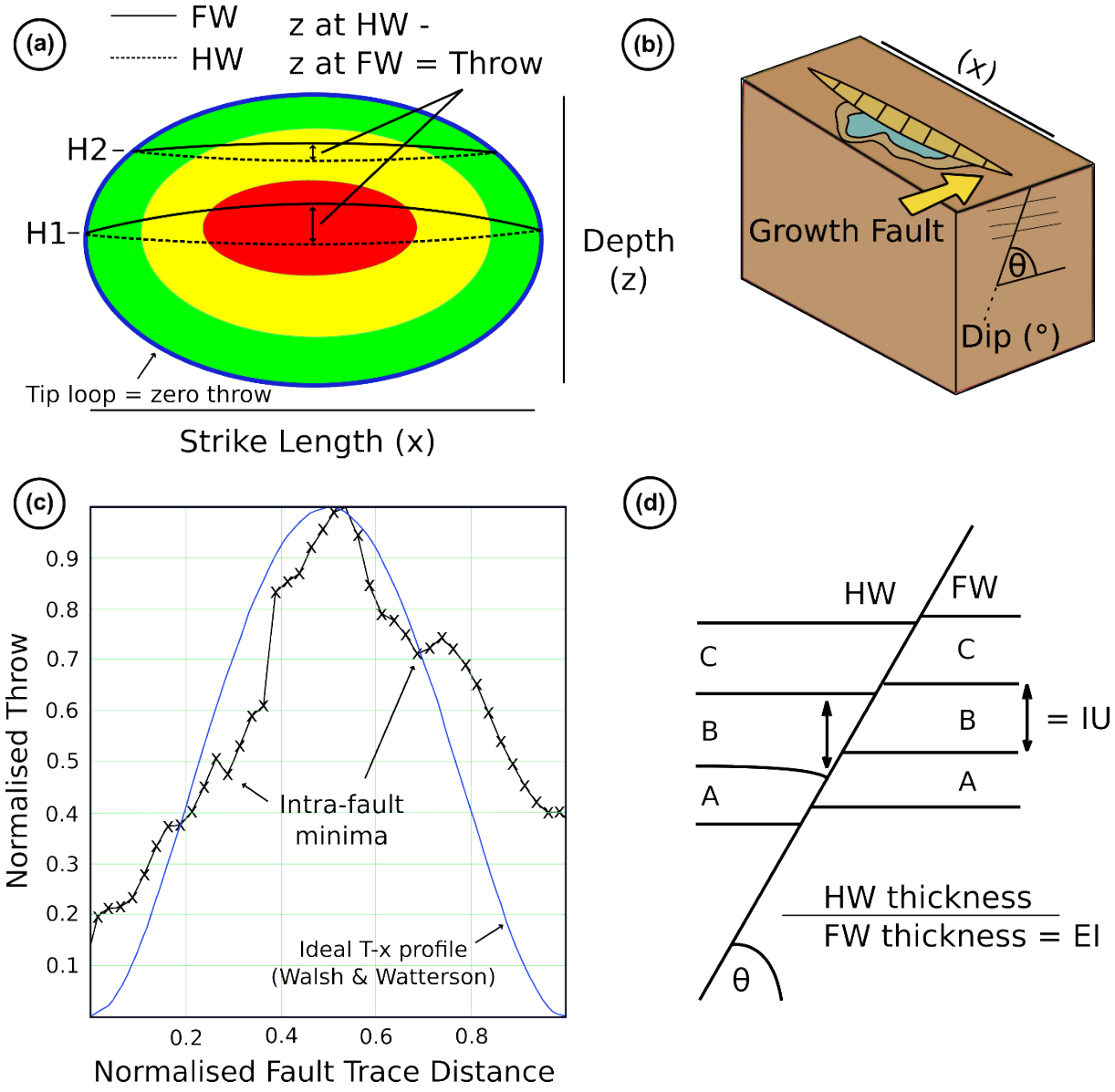

Figure 7. Illustration of fault terminology. (a) Definition of fault throw, displayed on an idealised fault plane, where throw occupies a finite strain envelope that reduces to zero at tips. (b) A growth fault breaching the free surface and influencing sediment dispersal. (c) Throw profiles for faults along strike. A fault used in the study is compared to an ideal fault displacement profile. (e) Growth faulting and stratal thickness. The thickness maps of Figure 10 are equal to the difference in depth between horizons. Expansion indices are calculated by dividing the hanging-wall thickness by the footwall thickness.

3.6.4 Expansion Index plots

Expansion index plots were used in this study to measure sediment accumulation in response to fault related subsidence and accommodation space creation. Faults that intersect the free surface and affect basin geometry and stratigraphic architecture are called growth faults (Childs, Nicol, Walsh, & Watterson, 2003). Large faults that intersect the free surface may accumulate thicker sedimentary successions in their hanging-wall depocentres (Figure 7d). If sediment supply remains constant or outpaces displacement rate, across fault thickening can be measured to constrain the duration of faulting. Expansion indices plots are constructed by dividing the hanging-wall thickness by the foot-wall thickness of a stratal unit across a growth fault (Cartwright, Bouroullec, James, & Johnson, 1998; Jackson & Rotevatn 2013; Thorsen, 1963). The resulting ratio of thickening records the initiation and cessation of faulting activity where ratios >1 indicate syndepositional fault growth. Measurements of thickness were made using seismic sections perpendicular to faults F1-F20 to measure the depths and thicknesses of horizons bounding EU1-EU10 (Figure 3b). Complications associated with the expansion index approach involve wall rock strain, differential compaction of footwall and hanging-wall strata, and incorrect correlation of seismic horizons (Jackson et al., 2017).

4. RESULTS

4.1 Fault Geometry

Depth structure maps of horizons H1-H4 indicate faulting is pervasive throughout the Sherbrook Supersequence within the survey area (Figure 8). Fault planes generally have along-strike lengths of 6-14 km and cuspate geometries with cylindrical profiles, and commonly feature convex corrugations at along-strike centres (Figure 6). All fault planes are generally curvilinear and planar-listric (Figure 6; 8). Throw, dip, strike and depth values for F1-F20 are presented in Table 2.

Table 2. Fault statistics for all faults in select arrays. Max. = Maximum Min. = Minimum

		Throw (m)		Dip (˚)		Strike (˚)		Depth (m)	
Array	Fault	Depth at Max.	Max.	Min.	Max	Min.	Max.	Min.	Max.
1	F1	3232	530	17	55	258	15	1894	5364
	F2	3177	560	9	59	241	32	1939	5627
	F3	3070	315	6	57	246	26	2045	5337
	F4	3253	459	13	58	219	43	2109	5006
2	F5	2889	318	15	57	266	341	1658	4128
	F6	2610	451	15	58	17	239	1736	5281
	F7	2787	245	16	50	259	14	1997	3995
	F8	3357	722	10	57	259	14	1694	6753
3	F9	2963	322	7	51	290	50	1538	4337
	F10	2643	167	19	55	334	55	2332	3539
	F11	2561	149	21	47	311	37	2046	3690
	F12	2854	220	27	60	357	65	1992	4288
	F13	3083	64	20	50	319	64	2512	3605
4	F14	2453	88	16	47	305	52	1696	3710
	F15	2759	162	32	55	352	40	2184	3477
	F16	2521	160	30	63	16	67	2003	3557
	F17	2648	177	18	54	347	40	2390	3508
	F18	2800	244	22	57	309	51	2062	4104
	F19	3032	115	26	52	18	77	2411	3593
	F20	2859	120	27	49	329	37	2141	3916

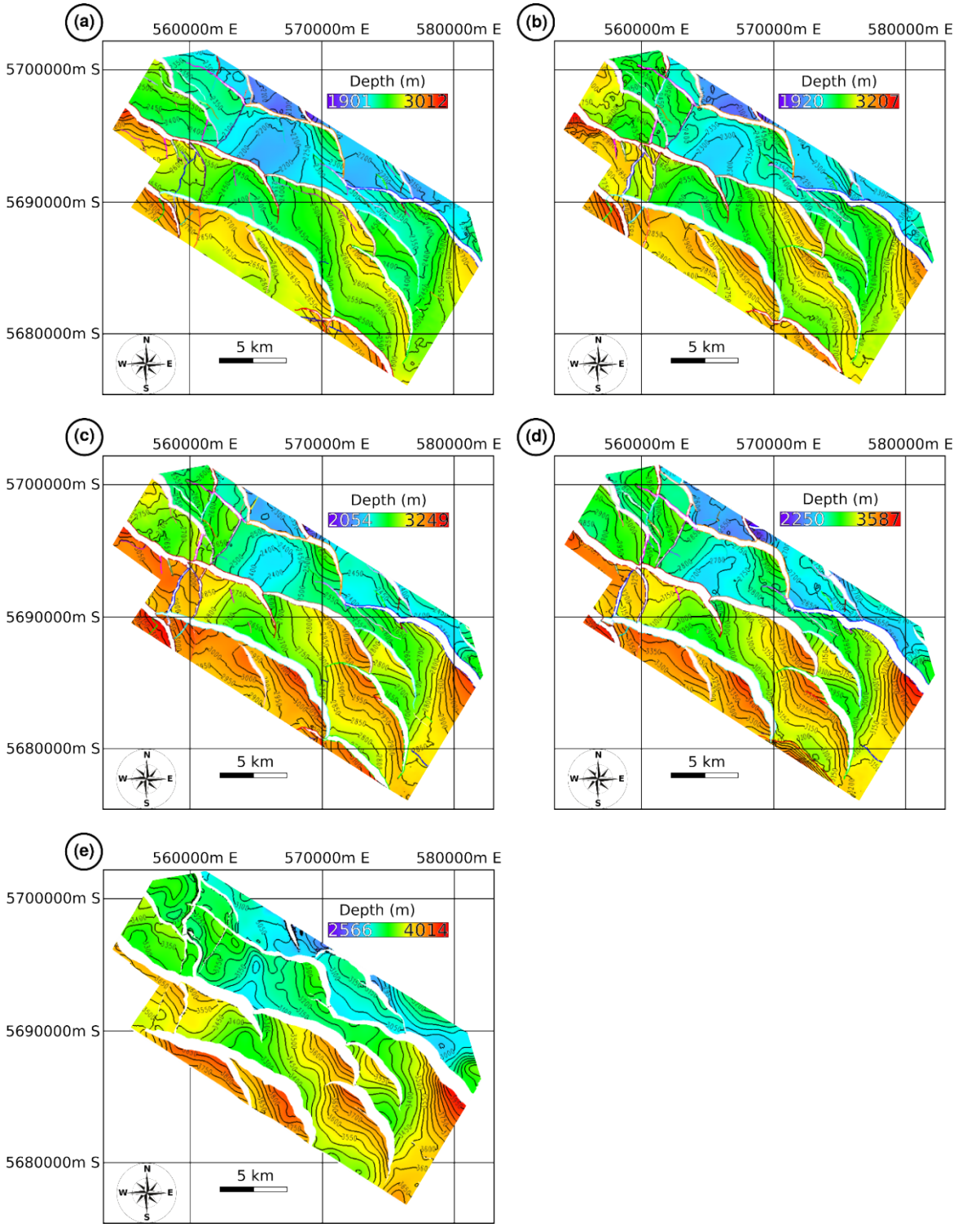

Figure 8: Depth structure maps of key horizons in the study area. (a) H5; (b) H4; (c) H3; (d) H2; (e) H1. Hotter colours indicate increasing depth. See Figure 3a for horizons relative to seismic and stratigraphic framework. Contour interval for all maps = 50m.

FA1

FA1 is composed of four NW-SE striking faults (F1-F4) that dip to the SW (Figure 5; Table 2). Strike lengths vary between 6-9 km (Table 2). All faults are listric in shape, with dips ranging from 6º for F1 to 59º for F2 (Table 2). The maximum vertical displacements on the faults (here called throw) range from 315 m at a depth of 3070 m for F3, to 560 m at depth of 3177 for F2 (Table 2). Faults F1-F4 offset horizons H1-H5 (Figure 8).

FA2

FA2 is composed of four NW-SE striking faults (F5-F8) that dip to the SW (Figure 5; Table 2). Strike lengths vary between 2-14 km (Table 2). All faults are listric in shape, with dips ranging from 10º for F8 to 58º for F6 (Table 2). The maximum vertical displacements of the faults range from 245 m of throw at a depth of 2787 m for F7 to 722 m of throw at a depth of 3357 m for F8 (Table 2). Faults F5-F8 offset horizons H1-H5 (Figure 8).

FA3

FA3 consists of five NNE-SSW striking faults (F9-F13) that dip steeply to the WNW (Figure 5; Table 2). Strike lengths vary between 2-4 km (Table 2). All faults are planar-listric in shape, with dip values that range from 7º for F9 to 60º for F12 (Table 2). The maximum vertical displacements of the faults range from 64 m at a depth of 3083 m for F13 to 322 m at a depth of 2963 m for F9 (Table 2). Faults F9, F11 and F12 offset horizons H1-H5. Fault F10 offsets horizons H1-H4, and F13 offsets horizons H2-H5 (Figure 8).

FA4

FA4 consists of F14-F20, seven NE-SW striking, NW dipping faults. Strike lengths vary between 2-5 km (Table 2). All faults are planar-listric in shape, with dip values that range from 16º for F14 to 63º for F16 (Table 2). The maximum vertical displacements of the faults range from 88 m at a depth of 2453 m for F14 to 244 m at a depth of 2800 m for F18 (Table 2). Faults F14 F16 and F18 offset horizons H1-H5. Fault F15 offsets horizons H3-H4, F19 and F20 offset horizons H2-H5, and F17 offsets horizons H2-H4 (Figure 8).

4.2 T-x analysis

FA1

Throw values are consistently larger at the stratigraphic level of H2 compared to H5 (Figure 9a). F1 possesses a significant throw minimum approximately at its along-strike centre. The position of the throw minima is a site of intersection with FA4. Throw broadly increases to the west where the remainder of the fault lies outside the limits of the survey area. F2 has a symmetrical bell-curve profile except for a sharp increase in apparent throw where F3 intersects the hanging-wall at H2, and a minimum throw values of ~150m at lateral tip points where F3 is linked along strike to F1 and F3 (Figure 9a). F3 has an even bell-curve profile except for a 20 m throw minimum at its along strike centre. Throw values reach low points at the southern tip and at the western tip a minimum of 100 m is reached where F3 links along strike to F2 (Figure 9a). F4 reaches throw values of 0 m at its lateral tip positions, an abrupt decrease in throw (~100m) at a position of intersection with F2, and a maximum throw

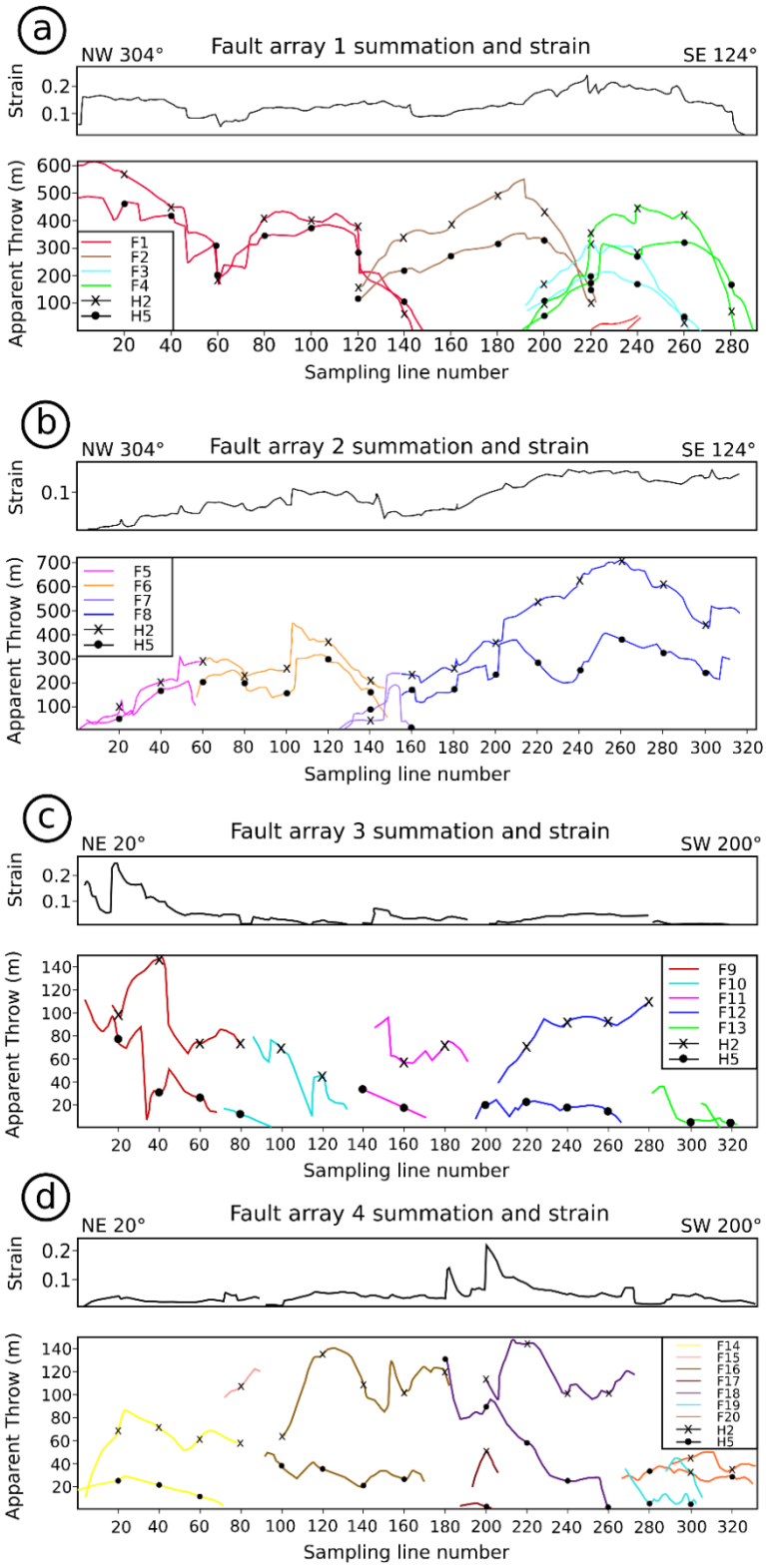

Figure 9. T-x plots for faults F1-4 (a), F5-8 (b) F9-13 (c), and F14-20 (d). The lower panel plots the apparent throws for these faults, that is, this is a T-x plot where throw at H2 and H5 is measured along strike of the fault array parallel to the average strike of the fault array. Individual faults in each array are coloured for identification, see Figure 6 for fault locations. The upper panel shows fault-related strain along the array, calculated as the sum of the apparent heaves divided by the pre-faulting line length across the fault.

of 450 m at its along strike centre (Figure 9a). Variations of apparent strike are otherwise gradual within FA1, except for the anomalous throw minima at F3 that is not associated with a linked fault or splay (Figure 9a). The strain of FA1 increases slightly towards the southeast and reaches a maximum of 0.22, where F2 and F4 intersect (Figure 9a).

FA2

Throw values for H2 are consistently larger than at H5 for all faults in FA2. F8 throw values are smallest at the point of linkage with F7 and increase gradually to the east. An abrupt decrease in throw is present at the western edge around sampling line number 300, for both H2 and H5 (Figure 9b). A low frequency throw minimum is present at sampling line 220-260 for H5 for F8. F7 has a max throw of 200 and abrupt decreases on either side of the maximum where F8 and F6 intersect F7 (Figure 9b). F7 throw values taper off at both lateral tips. F6 forms an intersection with F5 at sampling line 60, where F9 intersects and cuts across both the footwall and hanging-wall of F5 (Figure 9b). F5 reaches a minimum throw of 0m at the western end. F8 has the largest throw of FA2 (700 m at H2) and is responsible for most of the strain associated with FA2 (Figure 9b). A subordinate peak in strain values occurs at sampling line 100. Overall, strain increases to the SE end of the sampled area except for a minimum at sampling line 160 (Figure 9b).

FA3

Large differences between throw at H2 and H5 are present for all faults except for F9 (Figure 9c). Throw values at H5 do not exceed 40 m except for at the NE end of F2. F12

has a gradual throw profile with values increasing towards SW end (Figure 9c). Abrupt changes in throw area evident in F9, F10, F11 and F13 (Figure 9c). F9 reaches a maximum of 150m for H2 at sampling line 40. Most of the strain is associated with F9 and abruptly increases towards at the northern end of the sampled area (Figure 9c).

FA4

Apparent throw is consistently higher for H2 than for H5 in FA4 (Figure 9d). F18 has an asymmetric throw profile that increases from a value of 0 m at the SW tip to a maximum (130 m) at the NE tip for H5 (Figure 9d). At the level of H2, throw remains high at the SW tip, and reaches a maximum throw at the along-strike centre (140 m). F16 has two throw minimums either side of a peak around sampling line 160 (Figure 9d). Strain reaches a maximum near the centre of the sample grid and corresponds to elevated throw values of F18 and F17 (Figure 9d).

4.3 T-z analysis

FA1

T-z data for FA1 follow a D-shaped profile for all faults except F2, where a negative excursion occurs at a depth of 2600 m and throw reduces from 560 m to 350 m (Figure 10a). Throw values range between 200 m at a depth of 5500 m for F3, and 560 m at a depth of 2600 m for F2 (Figure 10a). Maximum throw values for the faults occur at a depth of 2400 m for F1, 3200 m for F2, 3200 m for F3, and 3350 m for F4 (Figure 10a). Minimum throw values occur at a depth of 5400 m for F1, 5750 m for F2, 5400 m for F3 and 5100 m for F4 (Figure 10a).

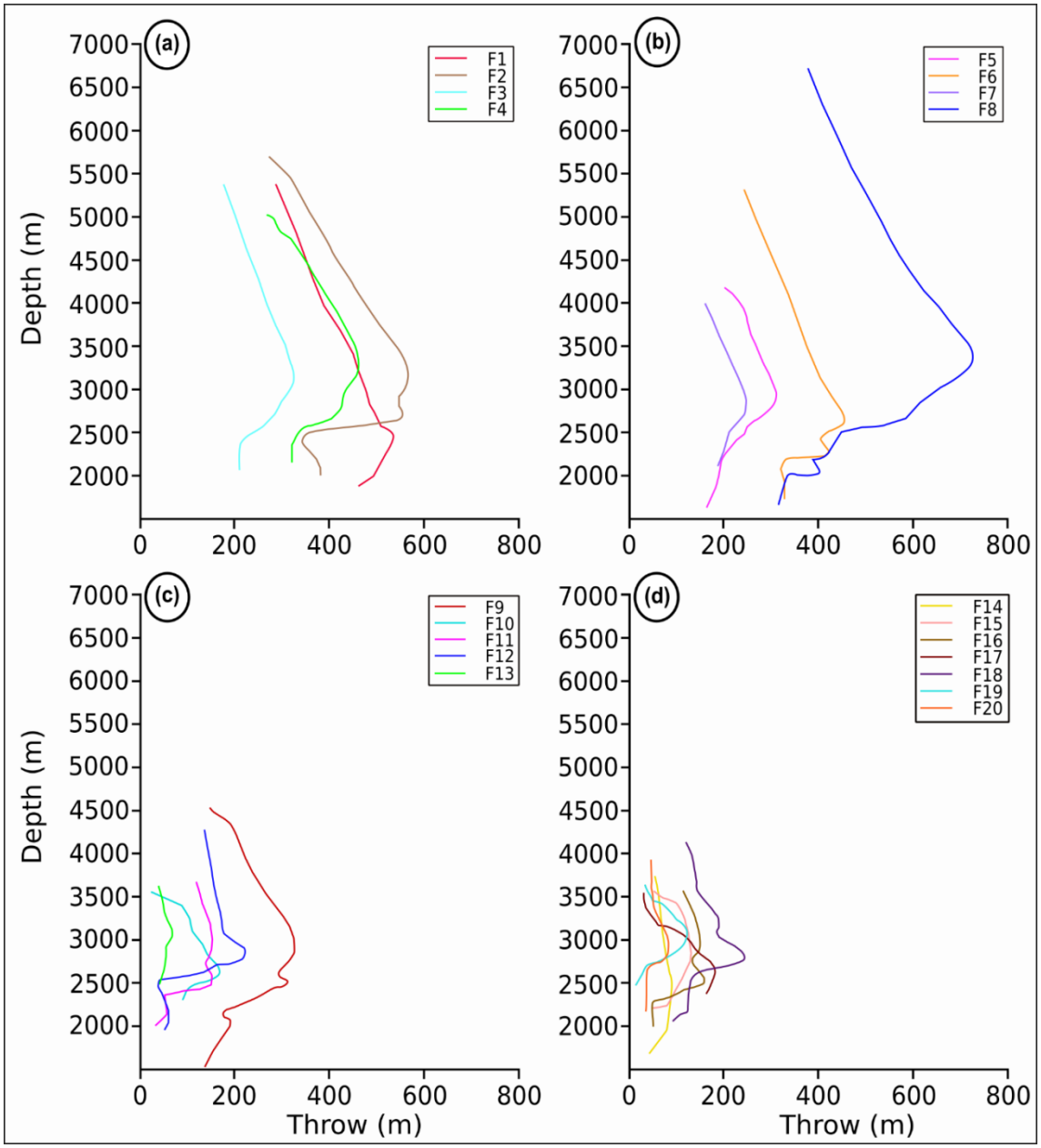

Figure 10. Throw-depth (T-Z) plots of maximum throw with depth along dip of fault planes. (a) FA1; (b); FA2; (c) FA3; (d) FA4. Individual faults in each array are coloured for identification, see Figure 6 for comparison. Throw values are based on intersection polygons for horizons shown on seismic sections in Figure 2a. See text for discussion.

FA2

T-z data for FA2 follow a smooth D-shaped profile for all faults except F6 and F8, where high frequency excursions are present between depths of 2000 m – 2500 m (Figure 9b). Throw values range between 180 m at a depth of 1600 m for F5 and 720 m

at a depth of 3400 m for F8 (Figure 10b). Maximum throw values for the faults occur at a depth of 2900 m for F5, 2650 m for F6, 2750 m for F7, 3300 m for F8. Minimum throw values occur at a depth of 1600 m for F5, 5250 m for F6, 4000 m for F7, and 1600 m for F8 (Figure 10b).

FA3

T-z data for FA3 follow a smooth D-shaped profile for all faults except F11 and F12 which have abrupt increases in throw between depths of 2400 m – 2500 m and 2500 m - 2600 m respectively (Figure 10c). Higher frequency excursions are present in F9 between depths of 2200 m and 2600 m (Figure 10c). Throw values range between 20 m at a depth of 3300 m for F10, and 320 m at a depth of 2900 m for F9 (Figure 10c). Maximum throw values for the faults occur at a depth of 2750 m for F9, 2600 m for F10, 3000 m for F11, 2800 m for F12, and 3100 m for F13 (Figure 10c). Minimum throw values occur at a depth of 5400 m for F1, 5750 m for F2, 5400 m for F3 and 5100 m for F4 (Figure 10c).

FA4

T-z data follow a smooth D-shaped profile for faults F14, F15 and F19. Throw at F16 increases abruptly between depths 2250 – 2500 m (Figure 10d). Throw values for F17 decrease with increasing depth (Figure 10d). Throw for F18 rapidly increases at depth of 2700m, and throw minima are present at 3100 m and 3600m for F18 (Figure 10d). Throw values range between 20 m at a depth of 2500 m for F19, and 250 m at a depth of 2750m for F18 (Figure 10d). Minimum throw values for the faults in FA4 occur at depths of 1700 m for F14, 2200 m for F15, 2000 m for F16, 3500 m for F17, 2100 m for

F18, 2500 m for F19, and 2200 for F20 (Figure 10d). Maximum throw values occur at a depth of 2500 m for F14, 2800 m for F15, 2600 m for F16, 2700 m for F17, 2800 m for F18, 3100 m for F19, and 2900 m for F20 (Figure 10d).

4.4 Isopach analysis

Isopach Unit 1

Stratal thickening is most prominent within hanging-wall depocentres of NW-SE striking faults toward the east of the survey area (Figure 11d). Stratal unit 1 reaches a thickness of 500 m in the hanging-wall depocenters of F3, F4 and F8, 20% greater than the thickness of nearby neutral areas distal from hanging-walls (400 m) (Figure 11d). A minimum of 300m thickness is within <1 km distance from a maximum ~480m near the hanging-wall of F5 (Figure 11d).

Isopach Unit 2

Stratal thickening is most prominent within hanging-wall depocentres at F2, F4 and F8, where thickness reaches 400 m, approximately 25% greater than average thickness of sediments distal to fault hanging-walls (Figure 11c). Thinning is pronounced at footwalls of F18 and F12, and at footwalls of F1 and F2 (~300 m). F2 and F4 together have increased and similar thickening in their hanging-walls (Figure 11c).

Isopach Unit 3

Stratal units thicken to 250 m at the western edge of the survey, in the hanging-wall depocentres of F1, F12 and F18 (Figure 11b), where thickness is approximately 60%

greater than the average thickness of 150m across the remainder of the study area (Figure 10b). Thickness reduced to 100 m at the footwall of F2 (Figure 11b).

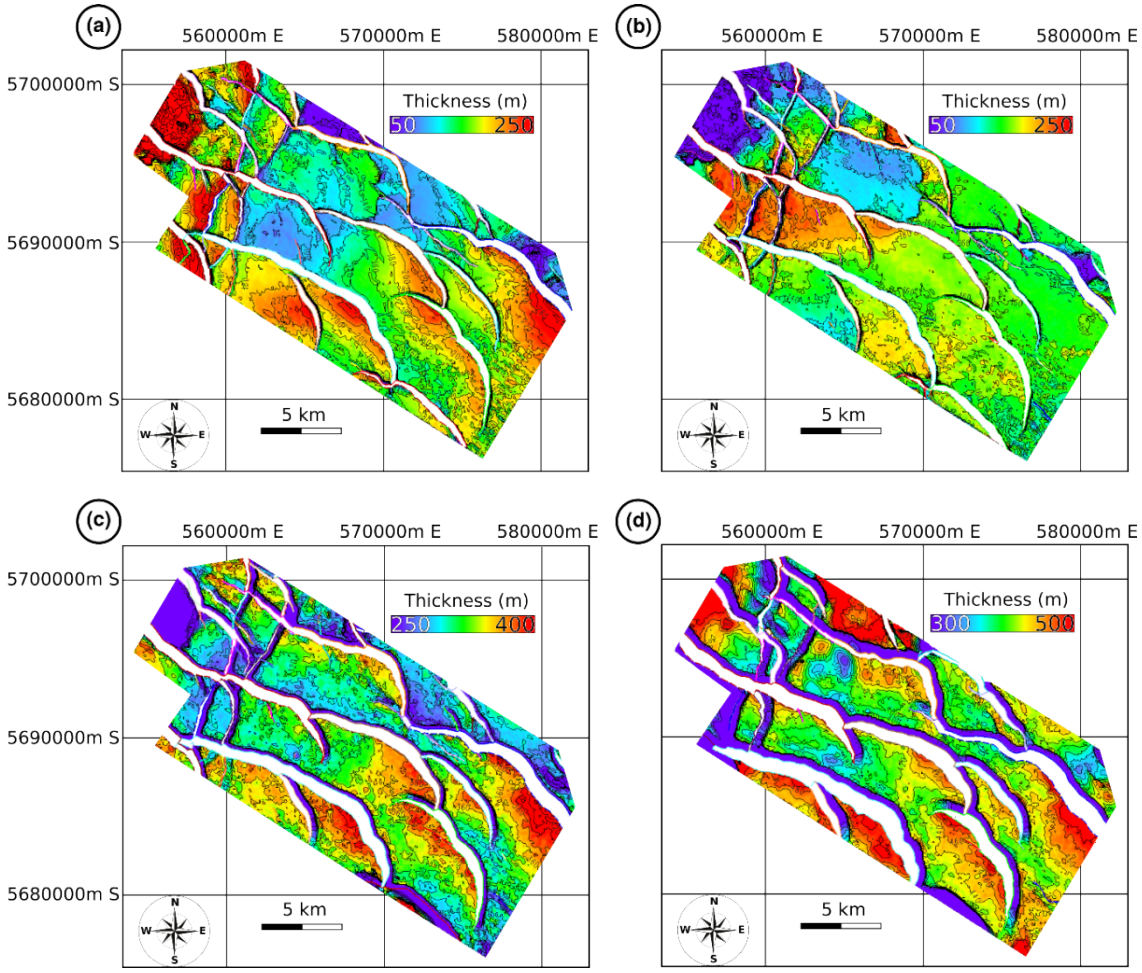

Figure 11. Isopachs of key stratal units within study area; (a) SU-4; (b) SU-3; (c) SU-2; (d) SU-1. Contour interval 20m. Hotter colours indicate areas of greater thickness. See Figure 4 for stratigraphic context of stratal units. Note the thickening of strata within hanging wall depocentres.

Isopach Unit 4

Stratal unit 4 thickens to 250 m at hanging-wall depocentres of F3, F4, and F8, and thin radially outwards to 150m thick at around 2km away from fault planes (Figure 11a). Stratal unit 4 thins to 100m on the hanging-wall block of fault 1, and in the area where F6, F7 and F8 link (Figure 11a).

4.5 Expansion index analysis

FA1

Expansion index values range between 0.7 and 2 for fault array 1 (Figure 12 a, b, c, d). Values are consistently >1 at EU-3, EU-5 and EU-10, and consistently <1 at EU-2. Expansion index values increase overall upward toward younger expansion index units (Figure 12 a, b, c, d).

FA2

Expansion index values range between 0.7 and 1.8 for fault array 2 (Figure 12e, f, g, h). Values are consistently >1 at EU-9 (Figure 12e, f, g, h). Expansion index values increase overall upward to toward younger expansion index units (Figure 12e, f, g, h).

FA3

Expansion index values range between 0.5 and 2 for fault array 3 (Figure 12i, j, k, l, m). Values are consistently >1 at EU-8, and consistently <1 at EU-9 (Figure 12i, j, k, l, m). Expansion index values decrease overall upward toward younger stratigraphic units.

FA4

Expansion index values range between 0.5 and 2 for fault array 4 (Figure 12n, o, p, q, r, s, t). Values are consistently >1 at EU-8 for all the faults (Figure 12n, o, p, q, r, s, t). Decreasing upward trends are present for all faults except for F15 (Figure 12n, o, p, q, r, s, t).

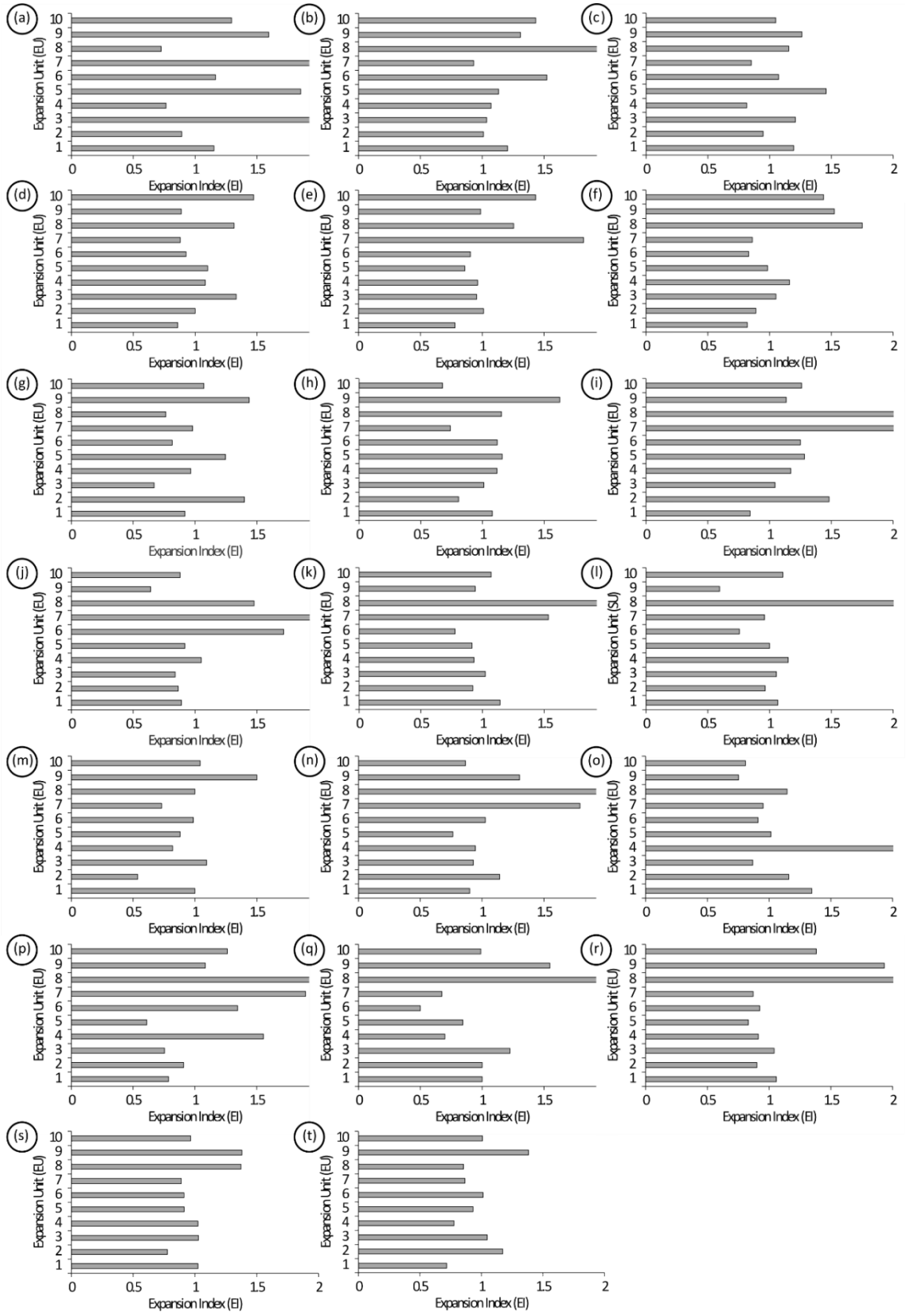

Figure 12. Expansion index plots for faults F1-F20. Expansion index is the calculated as the ratio of thickness of a hanging-wall layer compared to the same layer in the footwall (Figure 7d). EI calculated using EI units and horizons shown in Figure 3.

5. DISCUSSION

5.1 Geometry of faults

Faults in the western-central Otway Basin are the product of continental separation between Australia and Antarctica (Hill et al., 1995; Norvick & Smith, 2001). The faults in OS02-3D survey occupy a zone (Figure 13) characterised by a transition from orthogonal to obliquely rifted continental margin (Wilcox & Stagg, 1990; Stacey et al., 2013). During the Lower Cretaceous, N-S oriented rifting interacted with complex basement structures and resulted in E-W striking depocentres in the western and central Otway basin (Stacey et al., 2013). The first phase of Upper Cretaceous rifting (Turonian to Santonian) active in the deepwater Otway Basin resulted in deposition of the Shipwreck Supersequence (Figure 2) (Stacey et al., 2013). A second phase of Upper Cretaceous (Campanian to Maastrichtian) rifting resulted in deposition of the Sherbrook Supersequence (Figure 2, Figure 3) outboard of the Mussel-Tartwaup Fault Zone (Figure 1), which rotates clockwise to the SE where it merges with and Avoca-Sorell fault zone (Figure 1) (Stacey et al., 2013). Upper Cretaceous rifting is widely associated with other E-W and NW-SE trending faults in the Otway Basin generally (Finalyson et al., 1996; Perincek & Cockshell, 1994). In the OS02-3D survey area (Figure 1), prominent NW-SE striking faults of FA1 and FA2 offset the Sherbrook Supersequence (Figure 3, Figure 4, Figure 8) and have distinctly larger throw values and vertical extents than NE-SW oriented faults in FA3 and FA4 (Table 2). Andersonian fault theory (Anderson, 1951) states that normal faults form in response to gravitational stress (vertical), and have strike orientations perpendicular to the minimum tectonic (horizontal) stress. In the study area, prominent NW-SE striking faults in FA1 and FA2 (Figure 5a-b) have dip values up as steep 59º (Table 2) and are therefore interpreted as

listric-normal faults that formed during Upper Cretaceous (Turonian – Santonian and Campanian – Maastrichtian) NE-SW rifting, based on their strike and dip geometries.

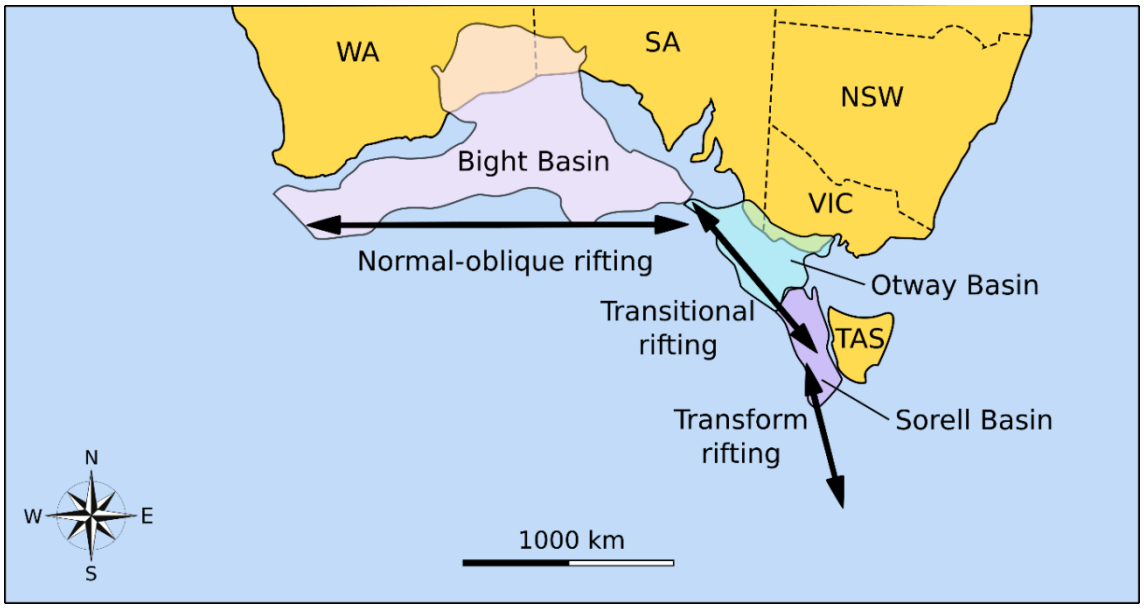

Figure 13. Southern margin rifting. Zones of normal-oblique rifting, transitional rifting, and transform rifting are indicated by black arrows. The adjacent Bight Basin is shown to the west, shaded pink. The Otway Basin is shown shaded green, and the Sorell Basin is shown in purple to the east.

Previously reported directions of extension during Upper Cretaceous rifting range from E-W to N-S (Hill et al., 1995; Moore, Stagg, & Norvick, 2000; Norvick & Smith, 2001; Totterdell et al., 2014). Varying extension directions may have therefore imparted an oblique-slip component during formation of F1-F8 (Wilcox & Stagg, 1990). Faults of FA3-FA4 dip WNW and have NNE-SSW strike orientations (Figure 6c-d; Figure 8a-e). Their orientation contrasts with the broad regional trend of NE-SW rifting and faulting in the Otway Basin (Hill et al., 1995; Moore, Stagg, & Norvick, 2000; Norvick & Smith, 2001; Wilcox & Stagg, 1990). Their NNE-SSW orientation is perhaps closely aligned with the orientation of the Avoca-Sorrell Fault Zone (Figure 1) (Gibson et al., 2013). The Avoca-Sorrell Fault Zone appears as a large westward dipping N-S striking

faults on deep crustal seismic cross sections across the study area (Finlayson et al., 1996, Moore et al., 2000). During Campanian-Maastrichtian rifting, faulting transitioned from the NW-SE Mussel-Tartwaup Fault Zone to the N-S Avoca-Sorrell Fault Zone during deposition of the Sherbrook Supersequence (Moore et al., 2000, Stacey et al., 2013). The importance of these basement structures and their reactivation on faulting in the western and central Otway basin has been proposed by Gibson et al. (2013), and faults within the OS02-3D seismic survey were proposed by Robson et al. (2016) to be formed via upward propagation and linkage to basement involved faults. Therefore, based on the geometries of F9-F20, FA3-FA4 are interpreted to be related to underlying basement structures of the Avoca-Sorrell Fault Zone and the transition from N-S rifting to E-W rifting (Hill et al., 1995; Moore, Stagg, & Norvick, 2000; Norvick & Smith, 2001; Totterdell et al., 2014).

Robson (2016) made comparisons to gravity driven faults in the adjacent Ceduna Sub-basin, where deltaic loading and shale detachment surfaces are proposed mechanisms of fault growth (Totterdell & Bradshaw, 2004). Correspondence between fault growth and deltaic loading of the Paaratte and Timboon sandstones is evident in this study as well (Fig 11; Figure 15). In the case of a gravity driven fault growth history, deltaic loading affects slope stability substantially and may induce faulting (Peel, 2014). Hall and Keetley (2009) demonstrated a transition from NE sourced deltaic loading to NW sourced deltas occurring during the Campanian (Figure 15). Strike-slip movement along crustal shear zones faults could be another possible mechanism responsible for nucleation of NE striking faults of FA3 and FA4. The Otway Basin occupies a proposed transition zone (Figure 13) between an oblique-normal N-S rifted margin segment to the

west of the Otway Basin and a transform NW-SE to NE-SW rifted segment to the east of the Sorrel Basin (Gibson et al., 2013; Stacey et al., 2013). Basement structures such as the Coorong Shear-zone and the Avoca-Sorrel fault zones are present in the study area and appear as large westward dipping fault systems on deep crustal seismic cross sections across the study area (Moore et al., 2000; Finlayson et al., 1996). I interpret that both mechanisms were important factors in the creation of NE trending faults. Fault growth for FA3 and FA4 is mostly stratigraphically constrained to a time after peak deltaic loading of the Paaratte Formation and before deposition of the overlying Timboon Mudstone (no offset), and have seismic characters that resemble starved sedimentary features suggesting deltaic loading caused abrupt faulting (Gawthorpe & Leeder, 2000). Their tendency to strike NE is controlled by underlying basement trends associated with oblique movement of the Coorong and Avoca-Sorrel fault zones. A cross-cutting relationship between FA1, FA2, and FA3, FA4 (Figure 7) implies the NE striking faults either grew contemporaneously with or prior to the prominent NW-SE trending faults (Figure 5). Reactivation of major NW-SE striking faults is evidenced by minor offset of post rift strata as young as the Cenozoic Nirranda Supersequence.

5.2 Growth of fault arrays

5.2.1 Lateral growth and linkage

Growth, segmentation and linkage of faults can be assessed via analysis of their throw variations (Baudon & Cartwright, 2008, Dawers & Anders, 1995; Robson et al., 2016). Growth and linkage of faults can be described in terms of the *'isolated fault model'* (eg. Cartwright, Trudgill, Mansfield, 1995; Walsh & Watterson, 1988) or the *'coherent fault*

model' (e.g. Walsh et al., 2003; Nicol et al., 2005 and Rotevatn, 2013). The isolated fault model (Figure 14a,d) proposes faults grow via synchronous increase of fault strike length and displacement, whereas in the coherent fault model faults establish their length early on and then accrue most of their displacement subsequently (Figure 14b,e) (Childs et al., 2017). A previous study by Robson et al. (2016) proposed that faults in the OS02-3D survey area probably grew in accordance with the isolated fault model, based on observations of variable throw along strike for faults equivalent to FA1 in this study. In this study T-x and T-z plots were constructed to assess segment and linkage both along strike and with increasing depth. The results of T-x analysis (Figure 7) reveal that faults exhibit mostly smooth bell-shaped profiles, except for abrupt throw variations that exist at points of fault intersection and interpreted linkage (Figure 7; Figure 9). An example of such abrupt changes of throw along strike is present at sampling line 190 of F2 (Figure 9a), where F4 intersects the hanging-wall of F2 (Figure 7e). Another example of abrupt throw increase occurs at sampling line 240 of F4 (Figure 9a), where a splaying fault intersects F4 at the stratigraphic level of H2. Throw values for individual faults gradually decrease toward points of intersection, e.g. F2 (Figure 9a). Strain values, however, do not exhibit minima at points of fault intersection (Figure 9a). Instead, the strain values vary gradually, suggesting faults may have grown in a kinematically coherent manner (Morley, 2017). Individual faults linked along strike at some point in time and formed arrays, however it cannot be determined how early linkage occurred, therefore either the isolated or coherent model may be applicable based on T-x analysis alone (Figure 9; Figure 14).

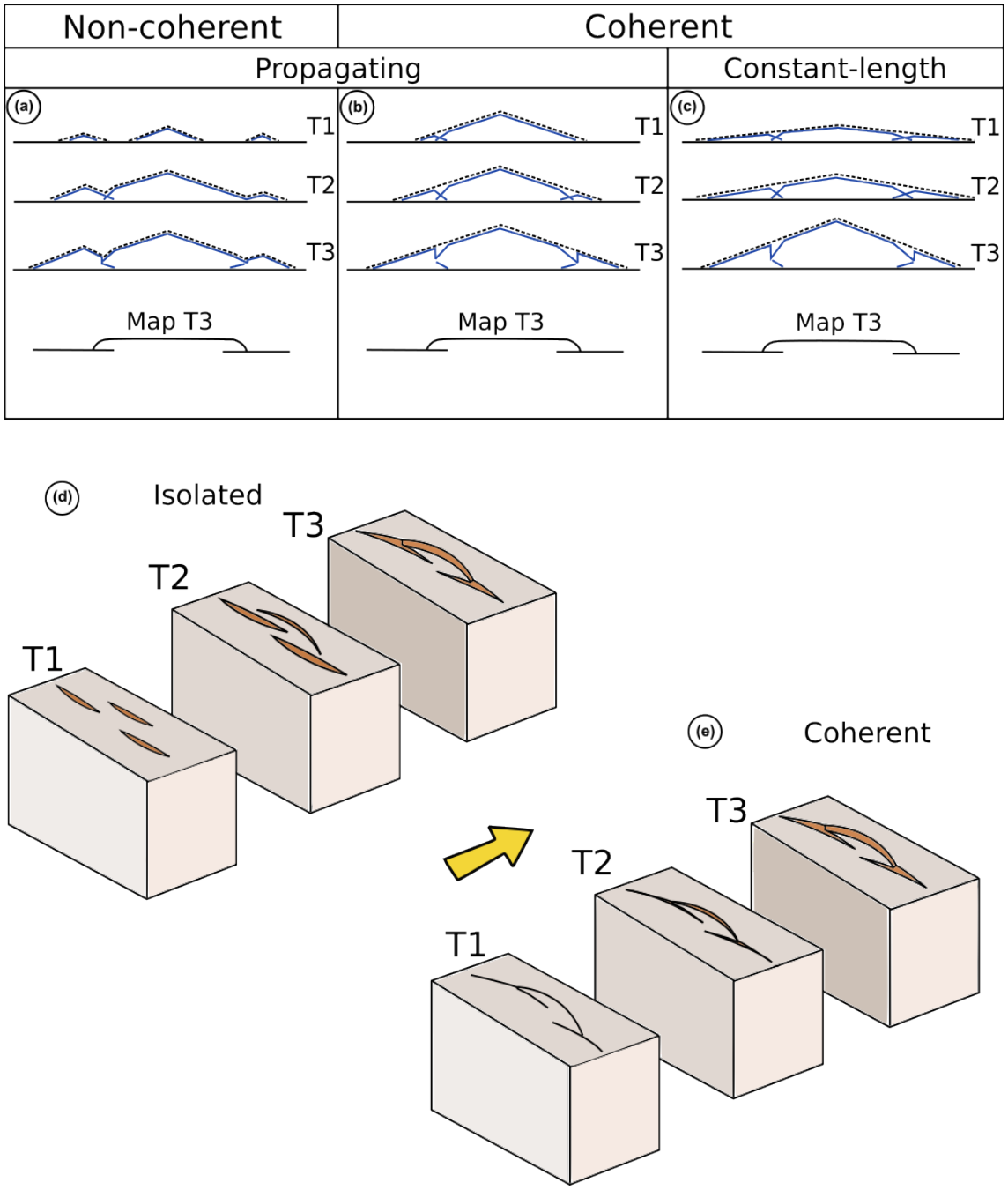

Figure 14: Schematic of the fault models, after Childs et al., 2019. (a) The propagating fault model, where individual faults at T1 begin to link at T2, and finally coalesce at T3. A perspective view of this process is shown at (d). (c) The constant-length model of faulting, whereby strike lengths are established early and subsequent fault growth is characterised by throw accrual. A perspective view of the coherent fault model is shown at (e).

At the stratigraphic level of H5, F8, a gradual decrease in throw is observed at the along-strike centre of the fault, where two individual faults potentially coalesced to

form F8 (Figure 9b). Isopach analysis reveals two points of thickening in IU-2 that are separated along strike within the hanging-wall of F8 (Figure 11c). In younger isopach units, these depocentres appear to grow along strike and coalesce, which may be evidence of fault growth in accordance with the isolated fault model (Jackson et al., 2017). Using isopach maps as indicators of kinematic activity relies on the assumption that thickness variations are fault related. Assumptions are invalid where point sourced sediments alter thickness, and where underfilled depocentres are filled subsequently after faulting (Jackson et al., 2017).

5.2.2 Vertical growth and linkage

Faults also exhibit linkage and growth in the vertical direction, referred to here as dip linkage (Mansfield & Cartwright, 1996). Throw variations along fault depth can be used to gain insight into fault reactivation, upward fault propagation, dip linkage and growth history (Baudon & Cartwright, 2008; Childs et al., 1996; Jackson et al., 2013; Robson et al., 2016). T-z plots constructed as part of this study (Figure 10) reveal broadly D-shaped throw profiles along depth with maximum throw values at depths between ~2500 m and ~3220 m, corresponding approximately to the stratigraphic level of H2 and H3 (Figure 7c-d). Abrupt decreases in throw occur upwards towards younger horizons, which may be due to lower shear strengths at shallower intervals inhibiting fault growth (Baudon & Cartwright, 2008). However, evidence of growth faulting and thickening of hanging-wall strata observed in isopach analysis (Figure 11) suggests faults intersected the free surface and controlled sediment dispersal (Gawthrope & Leeder, 2000; Jackson et al., 2017). Nonetheless, depths of observed maximum throw are likely points of fault nucleation and correspond to Turonian – Santonian ages,

consistent with the age of faults in the OS02-3D proposed by Robson et al. (2016), and the age of the first phase of Upper Cretaceous Turonian – Santonian faulting reported for the broader deepwater central Otway Basin region (Hill et al., 1995; Krassay et al., 2004; Stacey et al., 2013).

5.3 Evolution of fault arrays

Two phases of Upper Cretaceous faulting in the western and central Otway Basin were contemporaneous with deposition of the Sherbrook Supersequence (Stacey et al., 2013). The first phase of these phase is Turonian – Santonian age and the second phase is of Campanian-Maastrichtian age (Hill et al., 1995; Perincek & Cockshell., 1995). Isopach maps and Expansion indices measure thickness of fault related growth strata and may therefore constrain ages of faulting activity (Cartwright et al., 1998; Jackson & Rotevatn, 2013; Thorsen, 1963). Isopach maps reveal growth faulting for F2, F3, F4, F6, F8 was most active during deposition of IU-1 and IU-2, and most subdued during deposition of IU-3. While thickness of IU-3 is neutral within faults F2, F3, F4, F6, F8, prominent localised thickening >200m occurs within hanging-wall depocentres of F1, F12 and F18. During deposition of IU-4, growth faulting resumes at F2, F3, F4, F8 while moderate thickening occurs at F12 and F18. Ages of isopach units that exhibit growth faulting are consistent with two phases of faulting identified for the offshore central Otway Basin; Turonian – Santonian growth faulting corresponds to growth of IU-1 and IU-2, while Campanian – Maastrichtian growth faulting corresponds to growth of IU-4 following a phase of subdued faulting evident in IU-3. Predictions of fault growth based on synsedimentary growth packages is also based on the assumption that sediment supply is constant and associated faulting is growth faulting, i.e. faults breach

the free surface at time of deposition (Childs et al., 2003, Gawthorpe & Leeder, 2000). Results of EI analysis do present a clear trend to support conclusions derived from isopach analysis. Uncertainties may exist in the methodology due to data resolution, fault and horizon picking, and compaction. Since seismic data resolution decreases with depth, uncertainty in throw measurements increases with depth. Burial and compaction may result in lower measured throw values (Taylor, Nicol, & Walsh, 2008). Decompaction corrections were not applied since reliable lithology information was not available. A transition to NE-SW striking faults during deposition of SU-3 is evident, however the mechanism responsible for this event is uncertain. Faulting was either induced by sediment deposition and deltaic loading or driven by underlying basement processes (Avoca-Sorrel/Coorong Shear zone), or a combination of both.

5.4 Sediment transport

From the Turonian onwards, sequences in the Otway Basin became increasingly more marine until the Coniacian (Boyd & Gallagher, 2001). Facies maps of the Sherbrook Supersequence (Figure 15c-d) show that the survey area occupied a deep marine environment during Turonian deposition of the Flaxman and Nullawarre units (Hall & Keetley, 2009). A eustatic sea-level drop after the Coniacian resulted in a forced regression, and units of the Sherbrook Supersequence became more marine (Boyd & Gallagher, 2001). During the deposition of the Paaratte Formation, sediment transport changed direction and came from the NW (Figure 14b). During this time the OS02-3D area occupied a near shore environment (Boyd & Gallagher; Hall and Keeltey 2009).

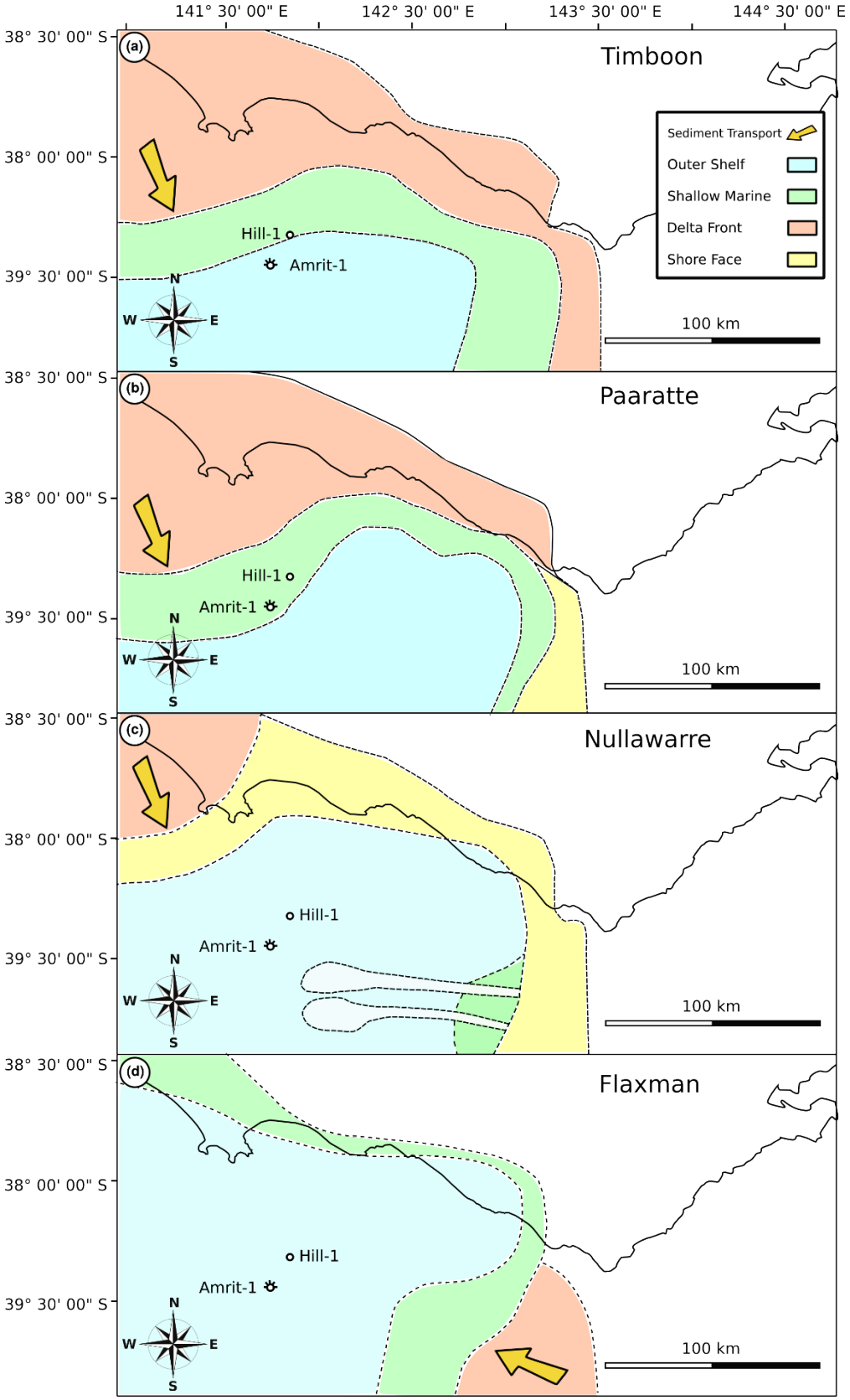

Figure 15: Facies maps for the Otway Basin, during deposition of the Timboon Formation (a), Paaratte Formation (b), Nullawarre Formation (e), and Flaxman Formation (d). Key legend shown top right. Direction of sediment transport indicated by yellow arrow.

A change in sediment transport direction as well as sudden deltaic loading above a marine mudstone coincides with a transition from NW-SE growth faulting to NE-SW faulting seen in IU-3 (Figure 11b). Similarities to gravity driven faults in the adjacent Ceduna Sub-basin were observed (Figure 13), however FA3 and FA4 were not included in this study by Robson et al. (2017). Hall and Keetley (2009) speculated a large NW-sourced sediment supply system was active as part of a large South Australian delta associated with an ancestral Murray River, related to uplift associated with Tasman Sea rifting and resulted in deltaic deposition that peaked during deposition of the Paaratte and Timboon Sandstone units approximately 80 Ma (Hall & Keetley, 2009). The relationship between faulting and sediment supply may an important factor controlling faults in the deepwater central Otway Basin, even though seismic facies commonly resemble that of a sediment starved basin in hanging-walls of FA3 and FA4.

5.5 Implications for hydrocarbon prospectivity

Poor fault-seal is an important risk factor for structural traps in the Otway Basin (Lyon et al. 2007; O'Brien et al., 2009; Stacey et al., 2013). The Otway Basin underwent persistent and pervasive reactivation throughout since the Eocene (Holford et al., 2011). In other areas of the Otway Basin, basement involved faults are associated with reactivation and secondary migration of hydrocarbons (Lyon et al. 2007). Traps in the Otway Basin bound by steeply dipping NW striking faults are at risk of reactivation and have poor seal potential due to associated escape pathways (O'Brien et al., 2009). Numerous potential structural traps are present within the OS02-3D survey at structural highs resulting from drag folding. Hanging-wall mudstones juxtapose tilted Paaratte Sandstone in the footwalls and form traps against NE striking faults. These faults are

less likely to have been reactivated due to their strike orientation. Offset is visible in post-rift strata as young as the Cenozoic in the study area. Some faults within the study area are linked in the dip direction to large basement involved faults (Robson et al., 2016). The results of this study therefore present a risk for hydrocarbon exploration in the study area.

Uncertainty regarding source rock potential presents another important risk in the region. Potential for hydrocarbon accumulations south of the shelf edge depends on charge from an unproven Turonian source rock or shallower source rocks of the Upper Cretaceous (Bernecker & Moore, 2003; Moore et al., 2000; O'Brien et al., 2007). Mehin and Link (1997) tested the potential for a source rock belonging to the unproven Austral-3 petroleum system. O'Brien et al. (2009) identified chemical traces of the potential source rock in nearby wells. Basin modelling has predicted the presence of oil prone generation window within the study area. The timing and displacement of faults analysed in this study may have implications for basin modelling of the deep-water Otway Basin.

5.6 Recommendations for further research

Correlation of deep-water facies with better known shelfal equivalents is difficult and due to limitations of available data would require a dedicated project to achieve accurate results. Our current understanding of stratigraphy in the deep-water Otway Basin is limited. Further studies in the deep-water regions of the Otway Basin would benefit from a revised adaption of the published lithostratigraphy and biostratigraphy to constrain and subdivide generic terms such as Belfast Mudstone into more constrained

units such as those proposed by Partridge (2001). Age constraints for deeper sequences would allow for more meaningful insights into the tectonic and structural evolution of the central Otway Basin. A thorough review of palynology in nearby wells followed by careful correlation using readily available seismic data together with findings of this study should achieve progress.

6. CONCLUSIONS

A detailed 3D model of the OS02-3D survey has been created, consisting of 5 key horizons and 20 seismic-scale faults. The style of faulting in the area is characteristic of multiple phases of rifting at oblique angles to basement structure, and interplay between sediment deposition and gravity driven faulting prevails. Structural analysis coupled with analysis of synsedimentary growth packages revealed the following:

(1) Two sets of faults are present in the OS02-3D survey area: [1] Turonian-Cenozoic NW-SE striking, SW dipping faults present throughout the Sherbrook Supersequence, and [2] smaller NE-SW striking, NW dipping faults restricted to the Paaratte Formation and the Timboon Formation.

(2) Growth faults actively controlled sediment dispersal since as early as the Turonian and resumed until Campanian-Maastrichtian times. Reactivation is apparent on larger faults displacing strata as young as the Paleogene.

(3) Deltaic loading and pre-existing structures at depth were important mechanisms responsible for faulting; and along with tectonic stresses controlled temporal evolution of faults. Pre-existing basement structures potentially influenced the strike orientation of faults.

(4) The structural evolution of faults in this study is consistent with the propagating fault model, whereby fault length growth is contemporaneous with accrual of fault throw, as opposed to the constant-length fault model, where fault length is established early in the faults life and does not increase with throw accrual.

ACKNOWLEDGEMENTS

Special thanks go to all whose knowledge and supervision have helped this project come to fruition. Dr. Rosalind King, my primary supervisor at the University of Adelaide, has patiently guided my efforts and made constructive suggestions throughout the year. Mark Bunch was a secondary supervisor at the Australian School of Petroleum and gave valuable feedback. Thanks go to Dr. Peter Boult Cooper Energy for Traptester training and mentorship during the course of this project. Additional thanks to Andy Foster and Amy Clarke at Badleys for Traptester support. Special thanks to all at Cooper Energy and the University of Adelaide for financial support and kind contributions to this project.

REFERENCES

ANDERSON, E. M. (1951). *The dynamics of faulting and dyke formation with applications to Britain*. Hafner Pub. Co..

BADLEYS T7 version 7.057 [Computer software]. (2019). Badleys Geoscience, North Beck House/North Beck Lane, Spilsby PE23 5NB, United Kingdom.

BAUDON, C., & CARTWRIGHT, J. (2008). 3D seismic characterisation of an array of blind normal faults in the Levant Basin, Eastern Mediterranean. *Journal of Structural Geology, 30*(6), 746-760. DOI: 10.1016/j.jsg.2007.12.008

BERNECKER, T., & MOORE, D. (2003). Linking basement and basin fill: Implications for hydrocarbon prospectivity in the Otway Basin region. *The APPEA Journal, 43*(1), 39. doi: http://dx.doi.org/10.1071/AJ02002

BOULT, P., FREEMAN, B., & YIELDING, G. (2016). Structural interpretation of seismic geologic reality, perspective, and 3-D thinking. In B. Krantz & C. Ormand (Eds.), *AAPG Memoir: Vol. 111. 3-D structural interpretation: Earth, mind, and machine* (pp. 75-89). American Association of Petroleum Geologists.

BOYD, G. A., & GALLAGHER, S. J. (2001). The sedimentology and palaeoenvironments of the Late Cretaceous Sherbrook Group in the Otway Basin.

BRIGUGLIO, D., HALL, M., & KEETLEY, J. (2015). Structural evolution of the Early Cretaceous depocentres, Otway Basin, Victoria. *Australian Journal of Earth Sciences, 62*(6), 717-733. doi: 10.1080/08120099.2015.1084048

CARTWRIGHT, J., BOUROULLEC, R., JAMES, D., & JOHNSON, H. (1998). Polycyclic motion history of some Gulf Coast growth faults from high-resolution displacement analysis. *Geology, 26*(9), 819-822.

CARTWRIGHT, J., & HUUSE, M. (2005). 3D seismic technology: the geological 'Hubble'. *Basin Research*, *17*(1), 1-20.

CARTWRIGHT, J. A., TRUDGILL, B. D., & MANSFIELD, C. S. (1995). Fault growth by segment linkage: an explanation for scatter in maximum displacement and trace length data from the Canyonlands Grabens of SE Utah. *Journal of Structural Geology*, *17*(9), 1319-1326.

CHILDS, C., HOLDSWORTH, R., JACKSON, C., MANZOCCHI, T., WALSH, J., & YIELDING, G. (2017). Introduction to the geometry and growth of normal faults. *Geological Society, London, Special Publications, 439*(1), 1-9. doi: http://dx.doi.org/10.1144/SP439.24

CHILDS, C., NICOL, A., WALSH, J., & WATTERSON, J. (2003). The growth and propagation of synsedimentary faults. *Journal of Structural Geology, 25*(4), 633-648.

DAVIES, R. J., STEWART, S. A., CARTWRIGHT, J. A., LAPPIN, M., JOHNSTON, R., FRASER, S. I., & BROWN, A. R. (2004). 3D seismic technology: are we realising its full potential?. *Geological Society, London, Memoirs, 29*(1), 1-10. doi: http://dx.doi.org/10.1144/GSL.MEM.2004.029.01.01

DAWERS, N. H., & ANDERS, M. H. (1995). Displacement-length scaling and fault linkage. *Journal of Structural Geology*, *17*(5), 607-614.

DUDDY, I., EROUT, B., GREEN, P., CROWHURST, P., & BOULT, P. (2003). Timing constraints on the structural history of the western Otway Basin and implications for hydrocarbon prospectivity around the Morum High, South Australia. *The APPEA Journal, 43*(1), 59-83. doi: http://dx.doi.org/10.1071/AJ02003

FINLAYSON, D.M, COCKSHELL, C.D, FINLAYSON, B, JOHNSTONE, D.W, REEVES, C.V, MORSE, M.P, & MILLIGAN, P.R. (1993). The Western Otway Basin ? a tectonic framework from new seismic, gravity and aeromagnetic data. *Exploration Geophysics, 24*(4), 493-500

FINLAYSON, D., JOHNSTONE, D., OWEN, A., & WAKEDYSTER, K. (1996). Deep seismic images and the tectonic framework of early rifting in the Otway Basin, Australian southern margin. *Tectonophysics, 264*(1-4), 137-152. doi: 10.1016/s0040-1951(96)00123-0

FREEMAN, B, YIELDING, G, & BADLEY, M. (1990). Fault correlation during seismic interpretation. *First Break, 8*(3), 87-95.

FREEMAN, BOULT, YIELDING, & MENPES. (2010). Using empirical geological rules to reduce structural uncertainty in seismic interpretation of faults. *Journal of Structural Geology, 32*(11), 1668-1676.

FREITAG, U., SANDERSON, D., LONERGAN, L., & BEVAN, T. (2017). Comparison of upwards splaying and upwards merging segmented normal faults. *Journal of Structural Geology, 100*, 1-11. doi: 10.1016/j.jsg.2017.05.005

GAWTHORPE, R., & LEEDER, M. (2000). Tectono-sedimentary evolution of active extensional basins. *Basin Research, 12*(3-4), 195-218.

GEARY, G., REID, I. S. A, & Victoria. Dept. of Natural Resources Environment. (1998). *Hydrocarbon prospectivity of the offshore eastern Otway Basin, Victoria, for the 1998 acreage release* (VIMP report ; 55). East Melbourne, Vic.: Dept. of Natural Resources and Environment. Retrieved: http://earthresources.efirst.com.au/product.asp?pID=559&cID=8&c=125830

GIBA, WALSH, & NICOL. (2012). Segmentation and growth of an obliquely reactivated normal fault. *Journal of Structural Geology, 39*, 253-267.

GIBSON, G., TOTTERDELL, J., WHITE, L., MITCHEL, C., STACEY, A., MORSE, M., & WHITAKER, A. (2013). Pre-existing basement structure and its influence on continental rifting and fracture zone development along Australia's southern rifted margin. *Journal Of The Geological Society, 170*(2), 365-377.

HALL, M. & KEETLEY, J. (2009). Otway Basin: stratigraphic and tectonic framework. *Geoscience Victoria 3D Victoria Report 2*. Department of Primary Industries.

HAZAR, M., TRUDGILL, BRUCE, SARG, FREDERICK, & SONNENBERG, STEPHEN. (2016). *The Tectonostratigraphic Evolution, Seismic Interpretation and 2D Section Restoration of the Offshore Eastern Otway Basin, Victoria, Australia,* ProQuest Dissertations and Theses.

HILL, K., COOPER, G., RICHARDSON, M., & LAVIN, C. (1994). Structural framework of the eastern Otway Basin: Inversion and interaction between two major structural provinces. *Exploration Geophysics, 25*(2), 79-87. doi: 10.1071/EG994079

HILL, K.A., FINLAYSON, D.M., HILL, K.C., & COOPER, G.T. (1995). Mesozoic tectonics of the Otway Basin region: the legacy of Gondwana and the active Pacific Margin – A review and ongoing research. *The APPEA Journal, 35*(1), 467.
DOI: http://dx.doi.org/10.1071/AJ94030

HOLFORD, S.P., HILLIS, R.R., DUDDY, I.R., GREEN, P.F., STOKER, M.S., TUITT, A.G., … MACDONALD, J.D. (2011). Cenozoic post-breakup compressional deformation and exhumation of the southern Australian margin. *The APPEA Journal, 51*(1), 613-638. https://doi.org/10.1071/AJ10044

HUANG, KE, ZHONG, GUANGFA, HE, MIN, LIU, LIHUA, WU, ZHE, & LIU, XUEFENG. (2018). Growth and linkage of a complex oblique-slip fault zone in the Pearl River Mouth Basin, northern South China Sea. *Journal of Structural Geology, 117*, 27-43. doi: 10.1016/j.jsg.2018.09.002

JACKSON, C. A., BELL, R. E., ROTEVATN, A. B., & TVEDT, A. (2017). Techniques to determine the kinematics of synsedimentary normal faults and implications for fault growth models. *Geological Society Special Publication, 439*(1), 187-217. doi:10.1144/SP439.22

JACKSON, C.A., & ROTEVATN, A. B. (2013). 3D seismic analysis of the structure and evolution of a salt-influenced normal fault zone: A test of competing fault growth models. *Journal of Structural Geology, 54*, 215-234. doi:10.1016/j.jsg.2013.06.012

KRANTZ, B., & NEELY, T. (2016). Subsurface structural interpretation: The significance of 3-D structural frameworks. In B. Krantz & C. Ormand (Eds.), *AAPG Memoir: Vol. 111. 3-D structural interpretation: Earth, mind, and machine* (pp. 91-109). American Association of Petroleum Geologists.

KRASSAY, A.A., CATHRO, D.L., RYAN, D.J. (2004). A regional tectonostratigraphic frame-work for the Otway Basin. In Boult, P.J., Johns, D.R., Lang, S.C. (Eds.), *Eastern Australasian Basins Symposium II* (pp. 97-116). Adelaide: Petroleum Exploration Society of Australia, Special Publication.

LAVIN, C J. (1998). Geology and prospectivity of the western Victorian Voluta Trough - Otway Basin for the 1998 acreage release. Victorian Initiative for Minerals and Petroleum. Report, (57), 63. Retrieved from http://earthresources.efirst.com.au/product.asp?pID=557&cID=8

LAVIN, C. (1997). The Maastrichtian breakup of the Otway Basin margin? A model developed by integrating seismic interpretation, sequence statigraphy and thermochronological studies. *Exploration Geophysics, 28*(2), 252-259.

LOVIBOND, R., SUTTILL, R., SKINNER, J., & ABURAS, A. (1995). The hydrocarbon potential of the Penola Trough, Otway Basin. *The APPEA Journal, 35*(1), 358.

LYON, P. J., BOULT, P. J., HILLIS, R. R., & BIERBRAUER, K. (2007). Basement controls on fault development in the Penola Trough, Otway Basin, and implications for fault-bounded hydrocarbon traps. *Australian Journal of Earth Sciences*, *54*(5), 675-689..,.

MANSFIELD, C., & CARTWRIGHT, J. (1996). High resolution fault displacement mapping from three-dimensional seismic data: Evidence for dip linkage during fault growth. *Journal of Structural Geology, 18*(2), 249-263.

MEHIN, K. & LINK, A.G., (1995). Early Cretaceous source rocks of the Victorian onshore Otway Basin. Victorian Initiative for Minerals and Petroleum Report 22. Department of Agriculture, Energy and Minerals.

MOORE, A., STAGG, H., & NORVICK, M. (2000). Deep-water Otway Basin: A new assessment of the tectonics and hydrocarbon prospectivity. *The APPEA Journal, 40*(1), 66. DOI: http://dx.doi.org/10.1071/AJ99005

MORLEY, C. K. (2017). The impact of multiple extension events, stress rotation and inherited fabrics on normal fault geometries and evolution in the Cenozoic rift basins of Thailand. *Geological Society, London, Special Publications*, *439*(1), 413-445.

NICOL, A., WALSH, J., BERRYMAN, K., & NODDER, S. (2005). Growth of a normal fault by the accumulation of slip over millions of years. *Journal of Structural Geology*, *27*(2), 327-342.

NORVICK, M.S, & SMITH, M.A. (2001). Mapping the plate tectonic reconstruction of southern and southeastern Australia and implications for petroleum systems. *The APPEA Journal, 41*(1), 15-35. http://dx.doi.org/10.1071/AJ00001

O'BRIEN, G., BOREHAM, C., THOMAS, H., & TINGATE, P. (2009). Understanding the critical success factors determining prospectivity—Otway Basin, Victoria. *The APPEA Journal,49*(1), 129. doi: http://dx.doi.org/10.1071/AJ08009

O'BRIEN, G.W. & THOMAS, J.H., (2007). A technical assessment of the yet-to-find hydrocarbon resource inventory, offshore and onshore Otway Basin, Victoria, Australia. Victorian Initiative for Minerals and Petroleum Report 90, Department of Primary Industries.

PALMOWSKI, D., HILL, K., & HOFFMAN, N. (2004). Structure and hydrocarbons in the Shipwreck Trough, Otway Basin: Half-graben gas fields abutting a continental transform. *The APPEA Journal, 44*(1), 417. doi: http://dx.doi.org/10.1071/AJ03016

PARTRIDGE, A. D. (2001). Revised stratigraphy of the Sherbrook Group, Otway Basin.

PEEL, F. J. (2014). The engines of gravity-driven movement on passive margins: Quantifying the relative contribution of spreading vs. gravity sliding mechanisms. *Tectonophysics*, *633*, 126-142.

PERINCEK, D., COCKSHELL, C.D., (1995). The Otway Basin: Early Cretaceous rifting to Neogene inversion. *The APPEA Journal, 35*(1), 451-466. doi: https://doi.org/10.1071/AJ94029

ROBSON, A., HOLFORD, S., KING, R., & KULIKOWSKI, D. (2018). Structural evolution of horst and half-graben structures proximal to a transtensional fault system determined using 3D seismic data from the Shipwreck Trough, offshore Otway Basin, Australia. Marine and Petroleum Geology, 89(3), 615-634.

ROBSON, A. G., KING, R. C., & HOLFORD, S. P. (2016). 3D seismic analysis of gravity-driven and basement influenced normal fault growth in the deepwater Otway Basin, Australia. *Journal of Structural Geology*, *89*, 74-87.

ROBSON, A. G., KING, R. C., & HOLFORD, S. P. (2017). Structural evolution of a gravitationally detached normal fault array: Analysis of 3D seismic data from the Ceduna Sub-Basin, Great Australian Bight. *Basin Research*, *29*(5), 605-624.

ROTEVATN, A., JACKSON, C., TVEDT, A., BELL, R., & BLÆKKAN, I. (2019). How do normal faults grow? *Journal of Structural Geology, 125*, 174-184. doi: 10.1016/j.jsg.2018.08.005

RYAN, S M, KNIGHT, L A, & PARKER, G J. (1995). The stratigraphy and structure of the Tyrendarra Embayment, Otway Basin, Victoria. Victorian Initiative for Minerals and Petroleum. Report, (15), 136. retrieved from http://earthresources.efirst.com.au/product.asp?pID=602&cID=8&c=14117

STACEY, A., MITCHELL, C., NAYAK, G., STRUCKMEYER, H., MORSE, M., TOTTERDELL, J., & GIBSON, G. (2011). Geology and petroleum prospectivity of the deepwater Otway and Sorell basins: New insights from an integrated regional study. *The APPEA Journal, 51*(2), 692. doi: http://dx.doi.org/10.1071/AJ10072

SUBRAMANIAN, R., 2005. Amrit-1 Interpreted Data Report. Santos Ltd report (unpublished).

TASSONE, D., HOLFORD, S., KING, R., TINGAY, M., & HILLIS, R. (2017). Contemporary stress and neotectonics in the Otway Basin, southeastern Australia. *Geological Society, London, Special Publications, 458*(1), 49-88. doi: http://dx.doi.org/10.1144/SP458.10 --- In geological settings

TAYLOR, NICOL, & WALSH. (2008). Displacement loss on growth faults due to sediment compaction. *Journal of Structural Geology, 30*(3), 394-405. Doi: 10.1016/j.jsg.2007.11.006

THORSEN, C. E. (1963). Age of Growth Faulting in Southeast Louisiana. Gulf Coast Association of Geological Societies Transactions Vol. 13 (1963), 103-110.

TOTTERDELL, J. M., BRADSHAW, B.E. (2004). The structural framework and tectonic evolution of the Bight Basin. In Boult, P.J., Johns, D.R., Lang, S.C. (Eds.), *Eastern Australasian Basins Symposium II* (pp. 41-61). Adelaide: Petroleum Exploration Society of Australia, Special Publication.

TOTTERDELL, J. M., HALL, L., HASHIMOTO, T., OWEN, K., & BRADSHAW, M. T. (2014). *Petroleum geology inventory of Australia's offshore frontier basins*. Geoscience Australia Record 2014/09. Geoscience Australia, Canberra.

TVEDT, A., ROTEVATN, A., JACKSON, C., FOSSEN, H., & GAWTHORPE, R. (2013). Growth of normal faults in multilayer sequences: A 3D seismic case study from the Egersund Basin, Norwegian North Sea. *Journal of Structural Geology, 55*(C), 1-20.

WALSH, J. J., BAILEY, W. R., CHILDS, C., NICOL, A., & BONSON, C. G. (2003). Formation of segmented normal faults: a 3-D perspective. *Journal of Structural Geology*, *25*(8), 1251-1262.

WILLCOX, & STAGG. (1990). Australia's southern margin: A product of oblique extension. *Tectonophysics, 173*(1-4), 269-281. doi: 10.1016/0040-1951(90)90223-U

YIELDING, G., & FREEMAN, B. (2016). 3-D seismic-structural workflows - examples using the hat creek fault system. In AAPG Memoir (Vol. 111, pp. 155-171). American Association of Petroleum Geologists.

APPENDIX A: EXTENDED METHODS

The data used for analysis and observation in this study is primarily derived from the structural and stratigraphic interpretation of a 3D seismic volume (OS02-3D).

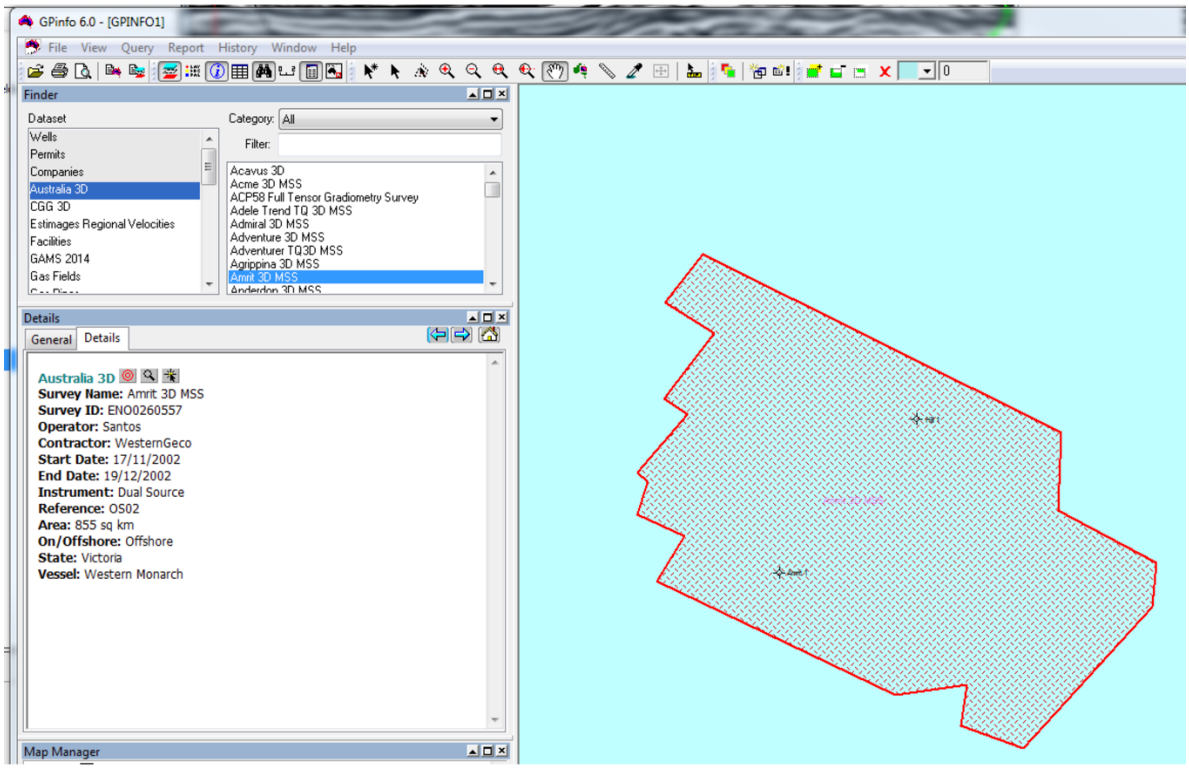

GPinfo source of Amrit 3D survey details.

The initial interpretation began with a Time volume. The data is loaded from a SEG-Y file that is available from a government database: http://er-info.dpi.vic.gov.au/documentation/srvy/os023d.htm.

Importing seismic and well data

A new project was created in Badley's Traptester v. 7.018.

SEG-Y amplitude data is loaded into Traptester as a time volume, and the survey definition is extracted from the volume extents in the SEGY Header.

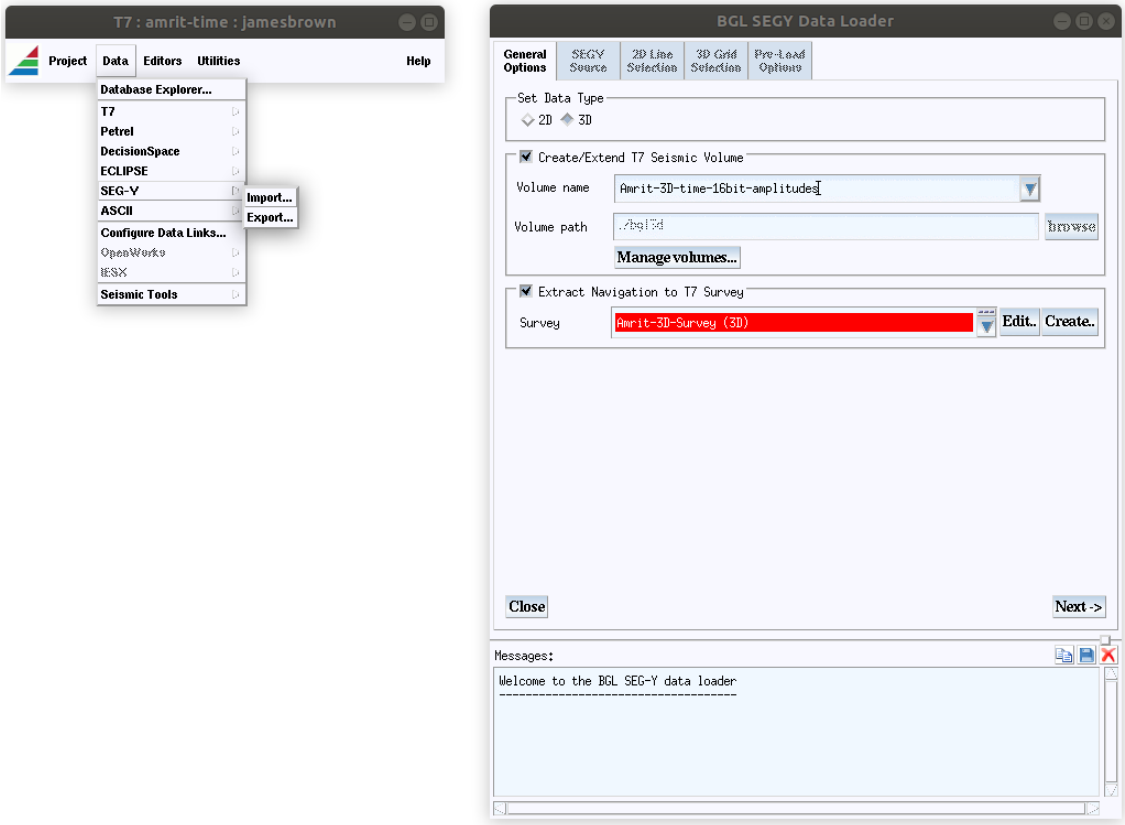

Importing seismic and from a segy file stored on the computer hard drive. The survey dimensions are extracted from the segy volume geometry.

Using the import > SEGY option from the Data tab in the main menu tool bar.

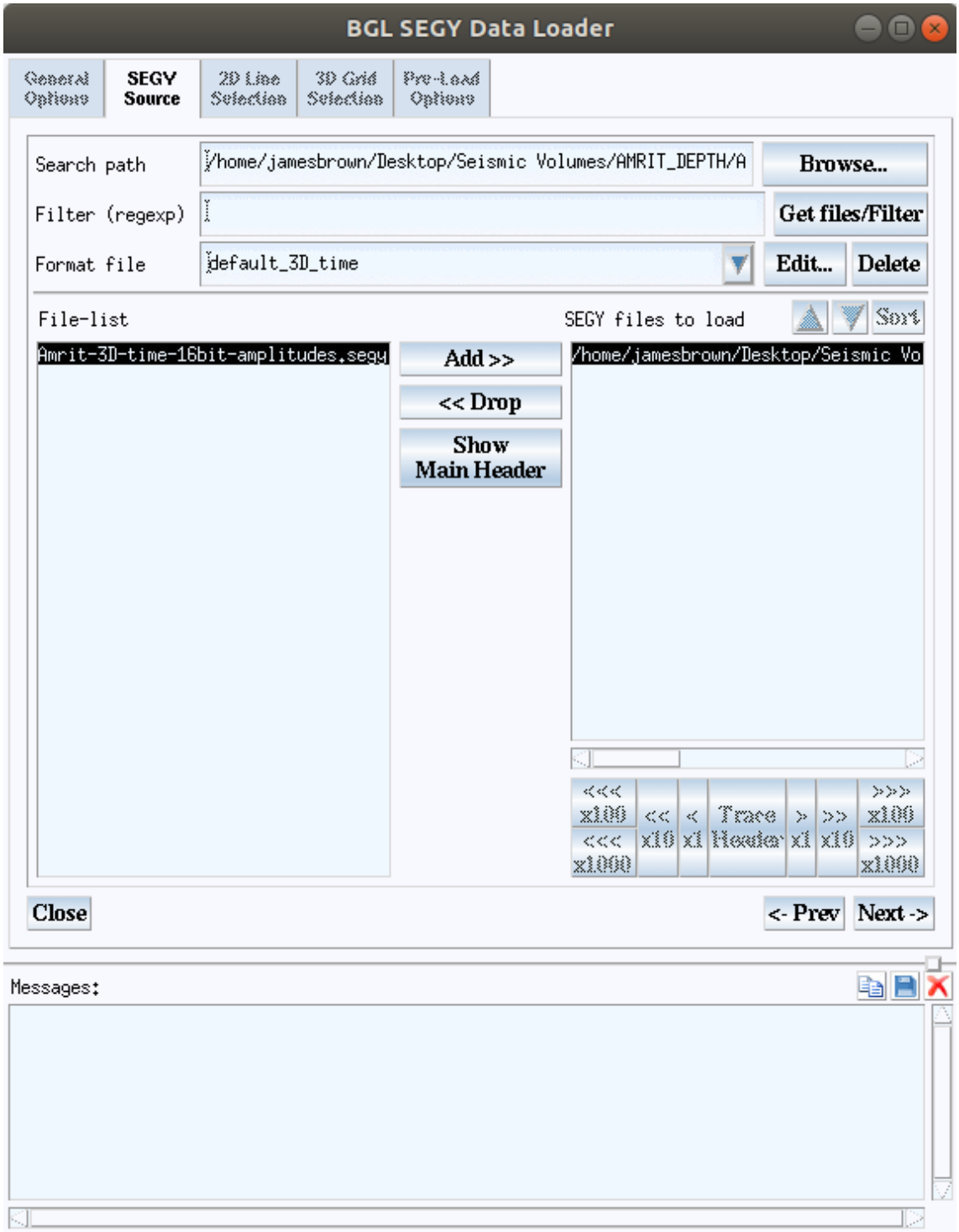

Segy selection and file format selection.

A folder containing the desired .segy file is selected, and one of the stock format files is selected to read the SEGY file.

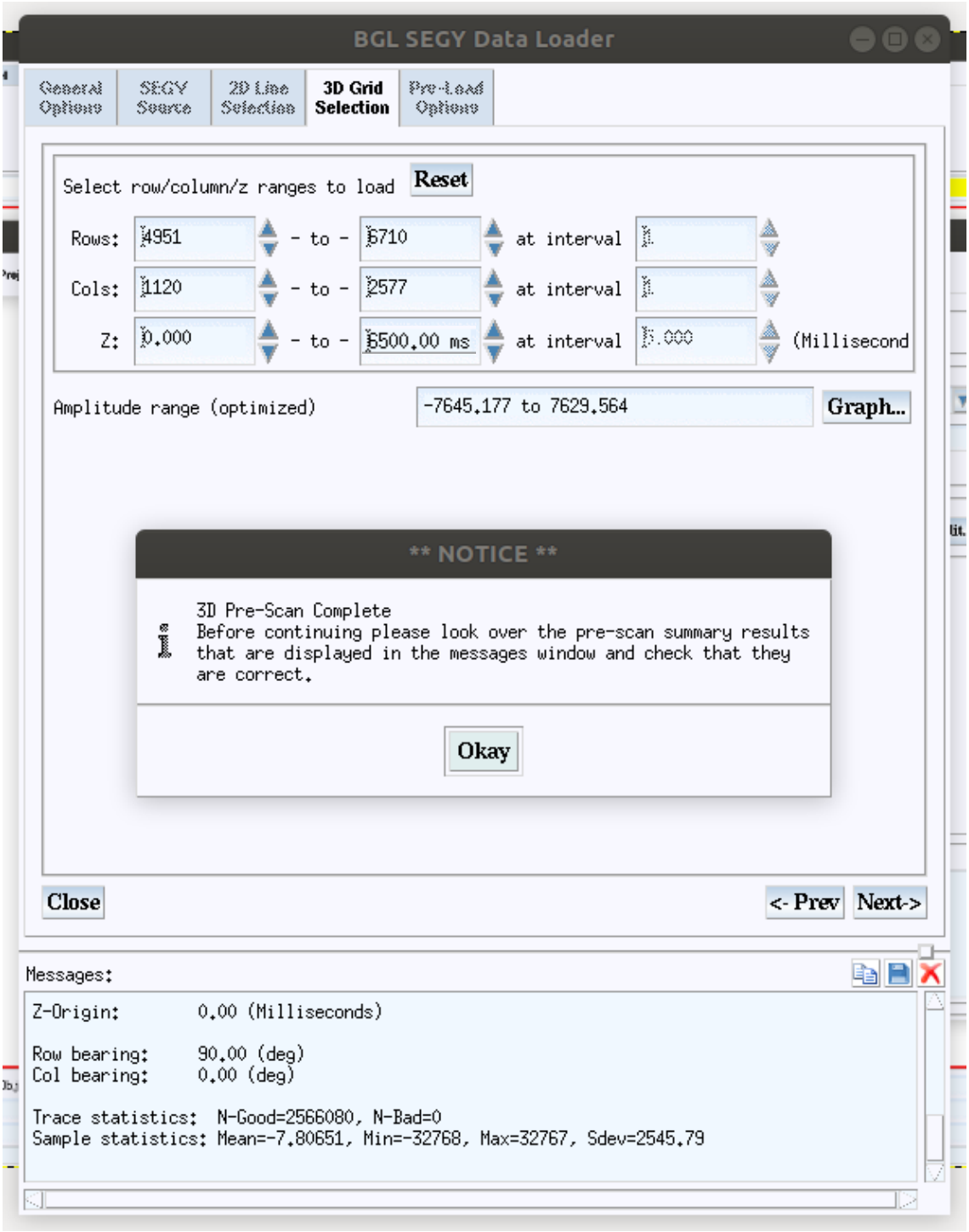

Pre scanned seismic volume with the above inlines and cross-lines imported.

Traptester performs a pre-scan to ensure that the in-lines, cross-lines, and depth are correctly extracted. The amplitude range is displayed. The pre-scan results should be checked to make sure the ranges are correct.

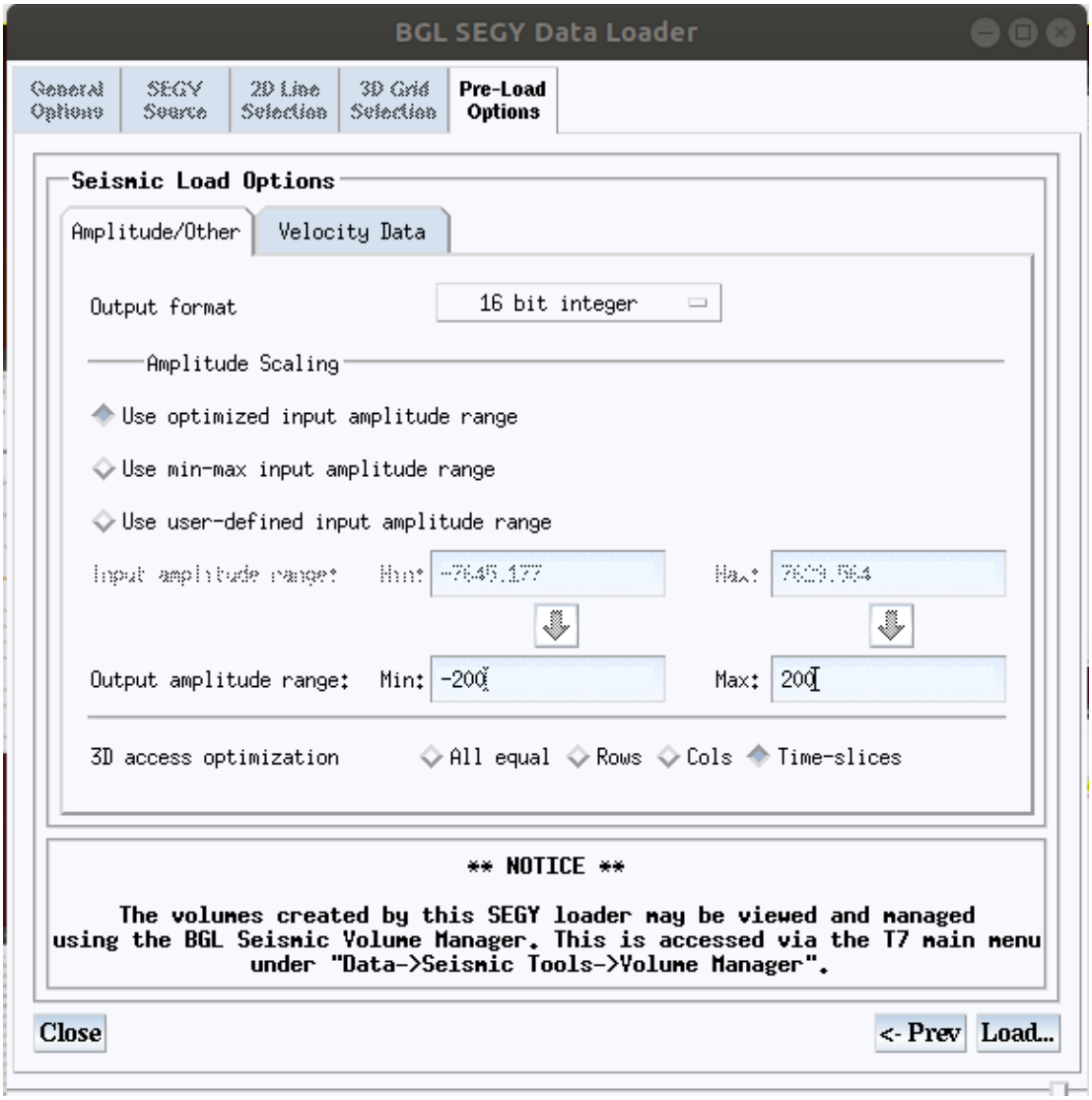

Setting output amplitude range and loading 3D seismic. Volume is optimised for time slices.

The output file is converted to a more efficient format that is used in the Traptester volume editor (BGL). The amplitude range can be scaled for the optimum contratst. The output format was set to 16 bit integer which ensures reasonable file sizes and quality.

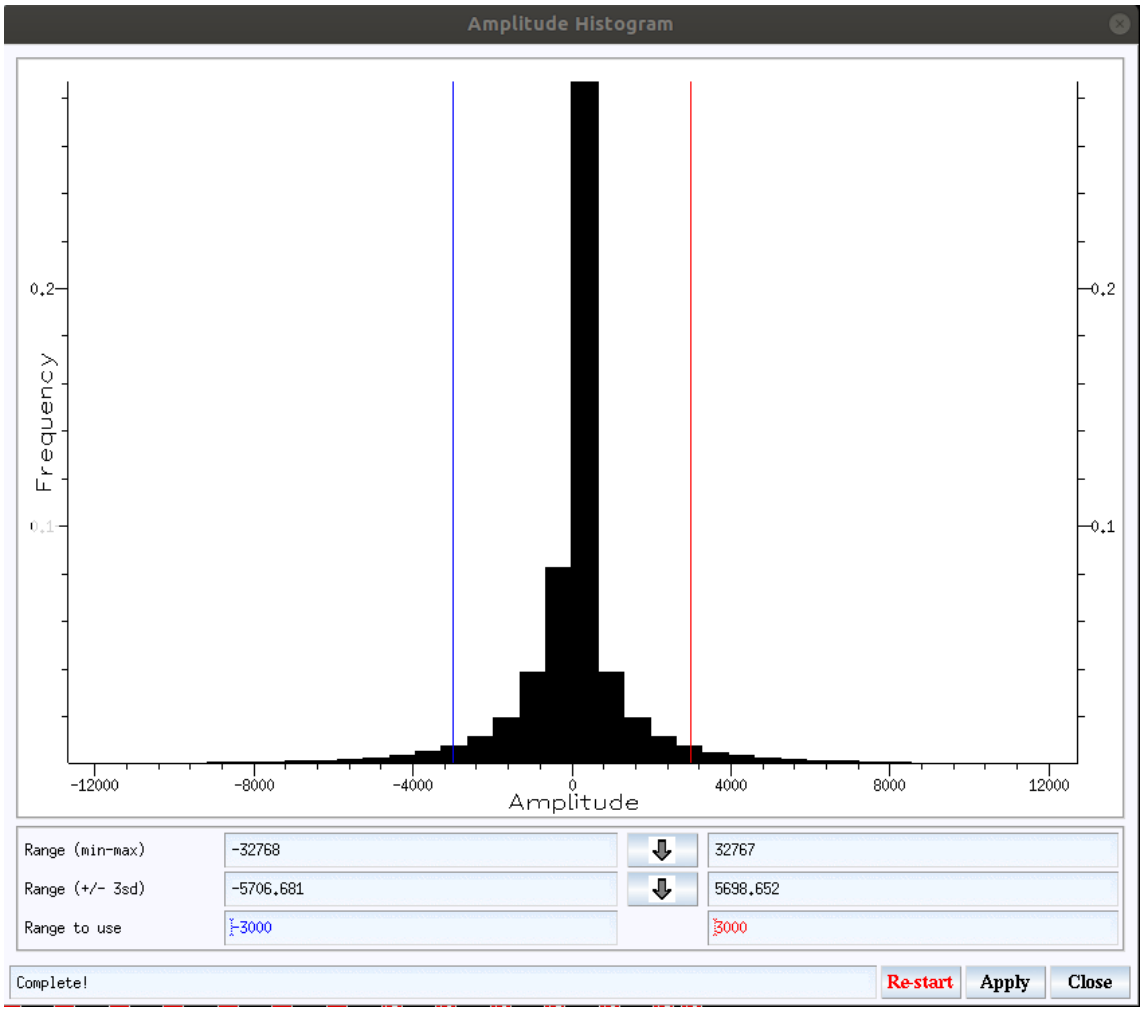

Amplitude histogram of amplitude depth data. The full range of data is cropped to remove noise and increase contrast in the range of interest, in this project cropped to between -3000 and 3000.

A histogram of the final volume with blue and red lines showing location of clip at minimum and maximum respectively.

FRAMEWORK CREATION

Creating fault surfaces

To begin building a framework model, unassigned fault segments are traced onto cross sections loaded in increments of 20. Since lines are spaced at 25m, the distance between interpreted sections is 500m. The Cross sections were first interpreted on columns, beginning in the west and proceeding in an Eastward direction. Once the entire area of the survey had been interpreted as accurately as is reasonable, the survey is interpreted again on rows, starting from the south and continuing northwards. Once the general trends in the fault segment raw data become apparent, more fault segments are picked on every 10th column/row (250m increments).

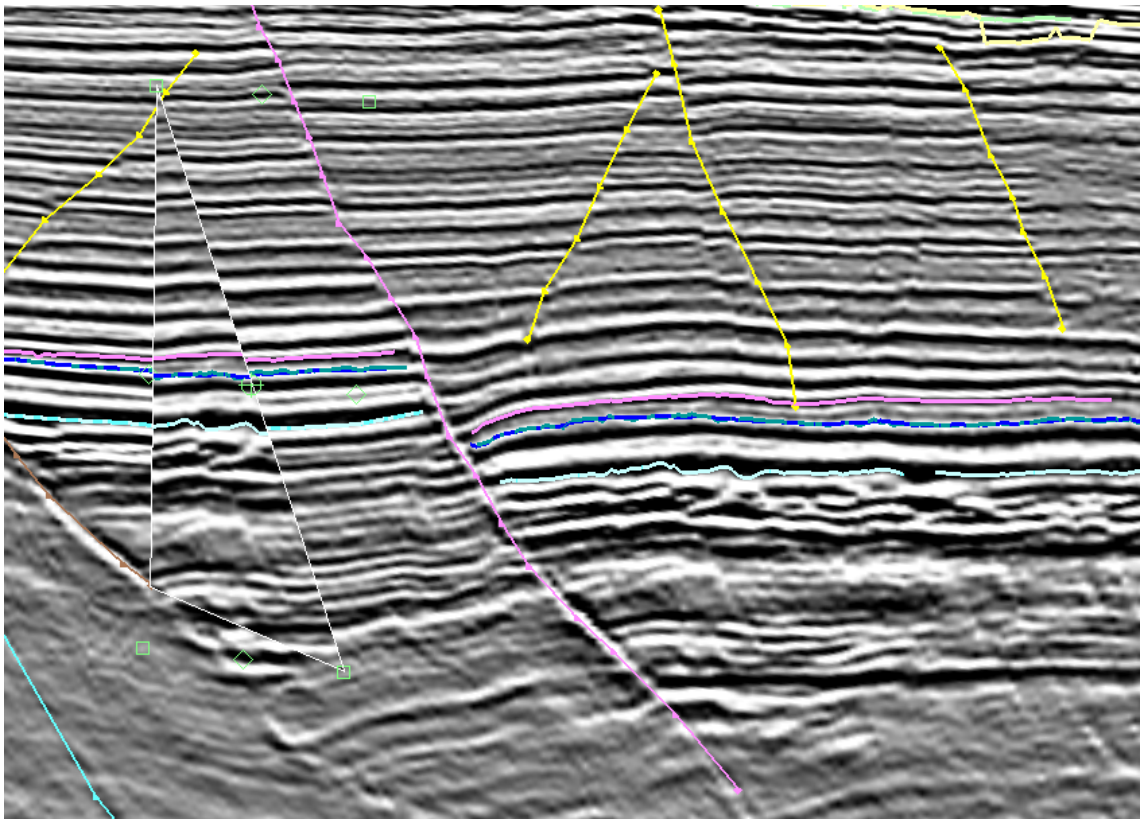

Seismic cross section, an inline selected from the OS02-3D survey with a pink fault segment, unassigned fault segments (shown in yellow) and horizon seed data shown in pink and blue.

The faults are picked where seismic reflectors are offset, usually at about 60º to horizontal in the case of normal faults. The horizons are picked along continuous reflectors between faults and are correlated across faults using the correlation panel to assess the seismic character of matching/same-age reflectors.

The fault segments are stored in the project database as unassigned segments that can be selectively assigned to a newly created fault. The process of selecting which fault segments belong to an interpreted fault is aided by the use of a correlation or coherency volume. A correlation/coherency volume is an attribute that amplifies discontinuities in seismic amplitude data and is especially useful for visualising offset of strata caused by faults. The creation of this correlation volume was performed in Traptester using the Volume Creation feature, using the Amrit time amplitude data as an input and selecting the correlation volume option as the output.

When loaded into the volume editor and positioned so that the tips of fault segments are exposed, the fault segments that intersect low coherence lines can be selected and assigned to individual faults.

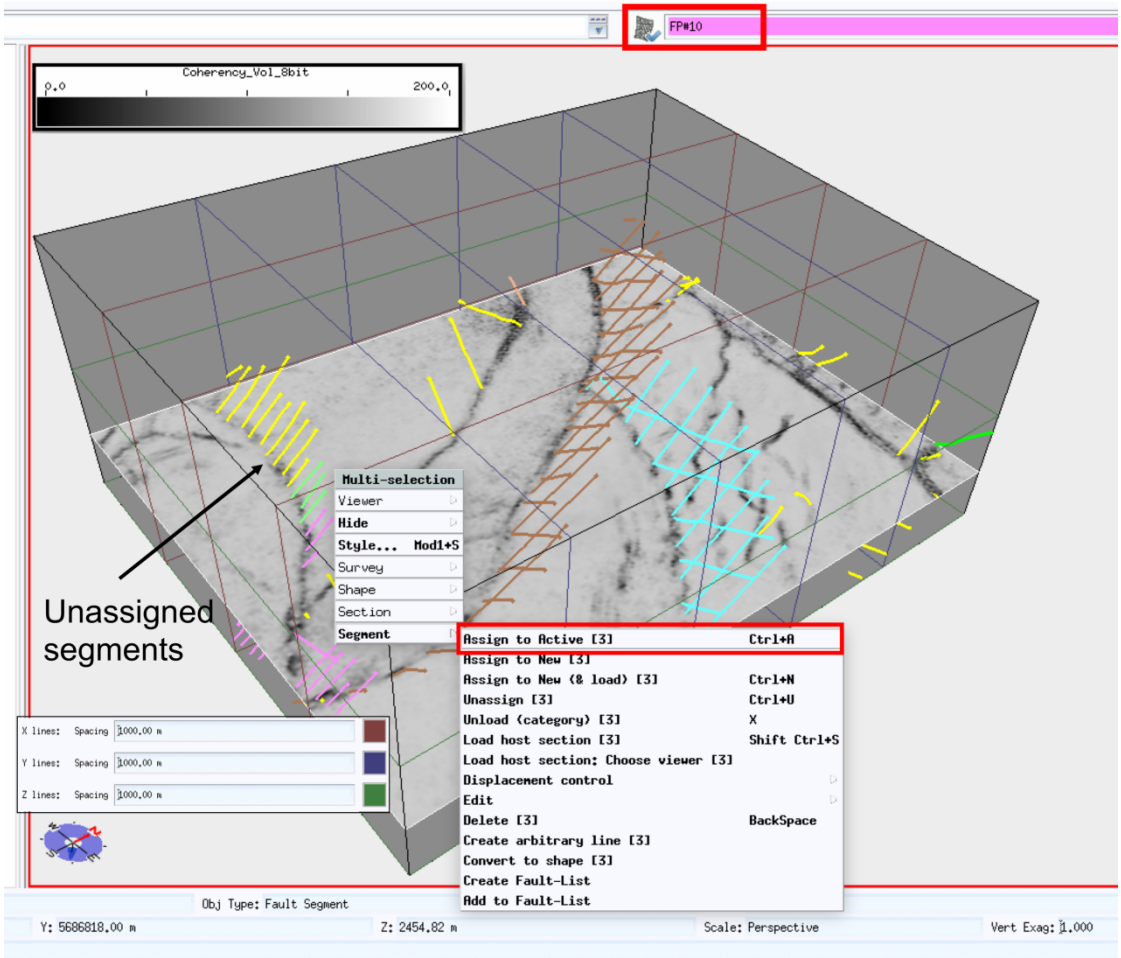

A coherency volume is used to highlight lineaments that are usually related to faults. These attribute volumes aid assignment of fault segments to individual faults.

Fault surface tri-meshes are then created from the assigned fault segments according to the fault surface modelling style selected in project parameters. In this case each fault surface is modelled using unconstrained triangulation for normal faults. This creates a surface composed of triangles with the shortest distance to fault segments. The smoothness of the data can be adjusting by selecting the maximum number of triangles that can be used to create the surface. The surface is then checked for quality. Accurate tracing of fault segments and correct designation of fault segments should result in smooth surface trimeshes/fault planes that are curvy planar in shape and quasi rectangular boundary profiles. Bumps in the trimesh are a result of inaccurately picked or incorrectly assigned fault segments. Fault segments are edited where necessary, and the surface tri-mesh is resynchronised with the fault segments until the fault surface resembles a fault plane.

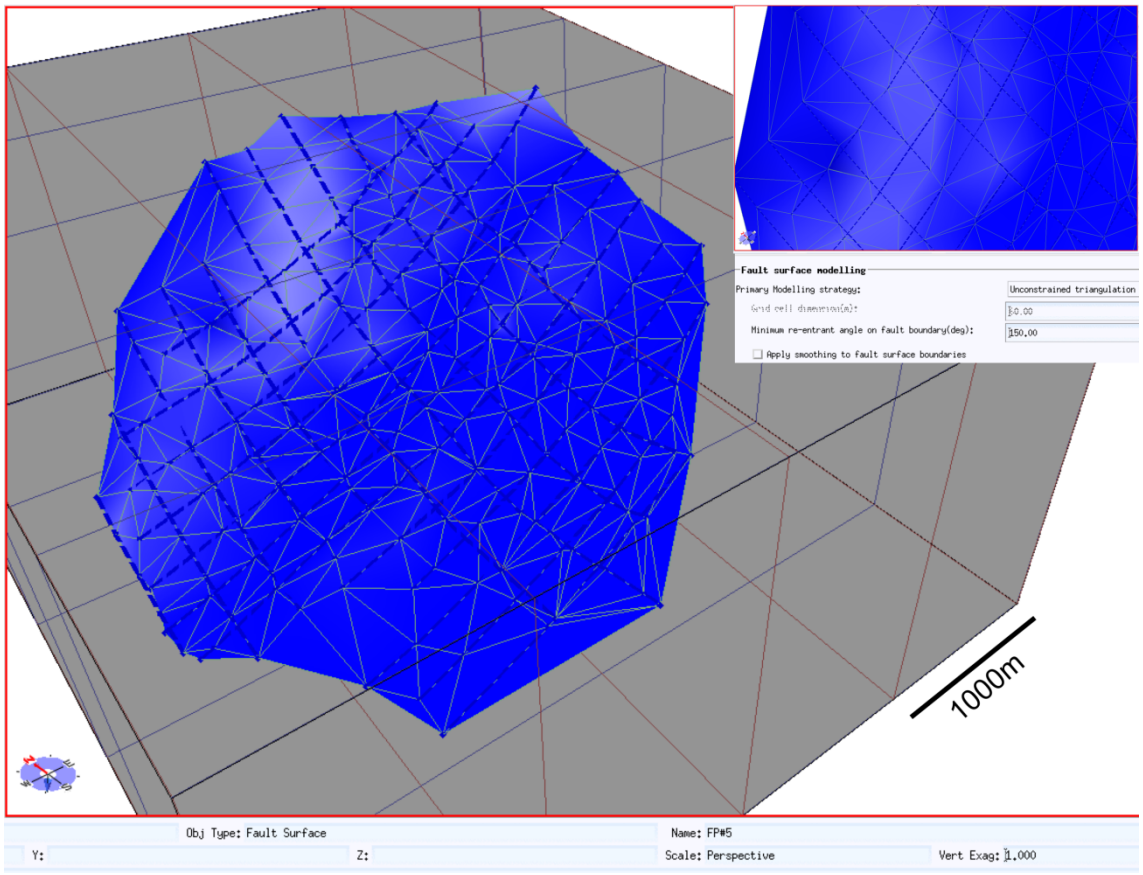

A triangulated fault. Triangles are shown taking shortest paths between points of fault segments. This display helps the interpreter to locate any anomalous bumps due to seismic or interpretation errors.

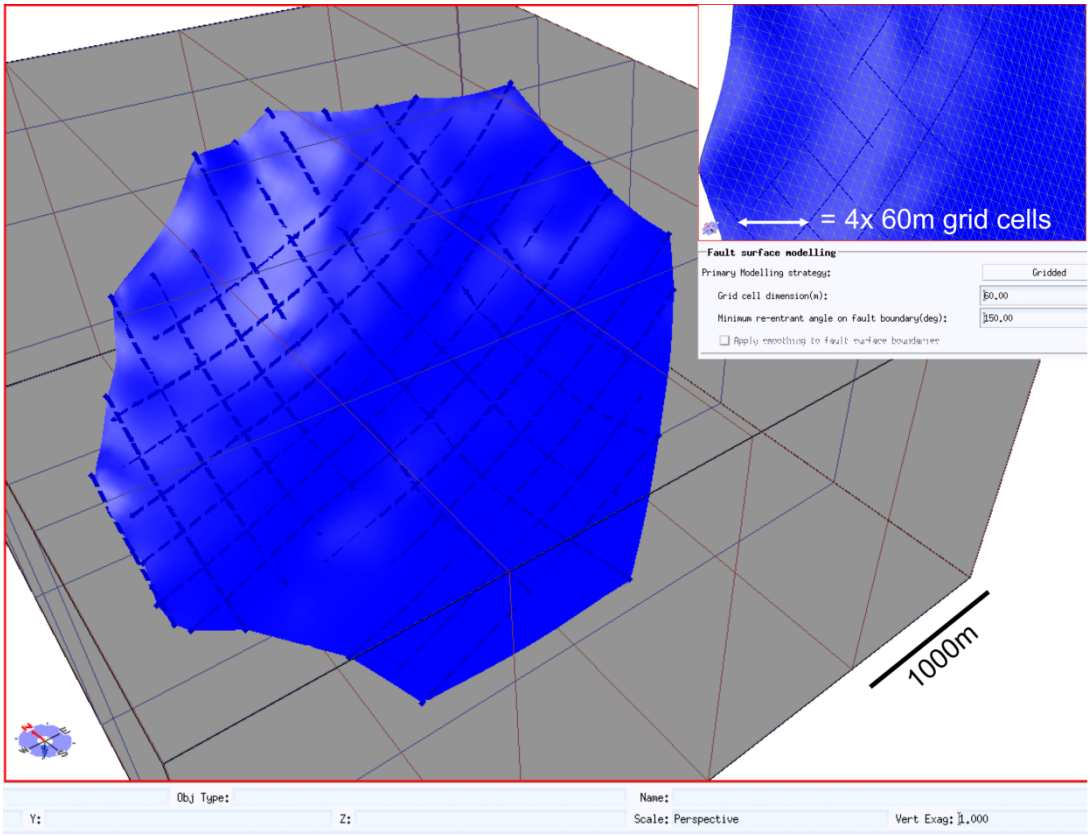

Gridded fault surface and with grid cell dimension set at 60m in project parameters, equal to approximately ¼ of the distance between fault segments.

There should be no overlap of fault planes, and faults that are interpreted as intersecting one another should be split and reconnected at branch lines. Branch lines are fault segments created on a fault surface which belong to another fault that intersects the fault hosting the branch line. Separate intersecting faults are selected as the splay and the master faults, for the purpose of joining the splay fault to the master fault at the location of the branch line hosted by the master fault surface.

Fault surfaces are then gridded after the rules above have been satisfied. Gridding is the process of interpolating fault raw data (segments) to create a best fit surface that honours the fault segments and results in a smooth fault plane. Grid cell dimensions determines the degree of smoothing of the data. Smaller grid cell dimensions demand more computation and result in more detailed surfaces. Larger grid cell dimensions are more expedient yet result in a smooth surfaces instead of honouring subtle/low frequency variations in fault segment geometries. It is recommend that the grid cell dimension need not be smaller than ¼ the distance between spacing between cross sections used to interpret fault raw data. In this study, fault segments were picked on every 10th line with 25m line spacings, therefore a grid cell dimension of 60m was used to model the faults.

Horizons

Using well tops from the Amrit Well completion report, the measured depths of the tops of major sequences were as follows:

Wangerrip: 2112 MD

Timboon Sandstone: 2383 MD

Paaratte: 2550 MD

Reflectors in between marker horizons were picked within the growth sequence based on continuity throughout the survey, even spacing, representation of pre, syn and post kinematic strata, stratigraphic importance, and hydrocarbon prospectivity (seal/reservoir contact etc.).

Seed Grid Creation

Horizons were created and seed volumes assigned to the respective horizons are picked on an arbitrary line that intersects the well. The frame controller was used to slowly grow the interpretation towards the survey edges, starting near the well. Cross sections are initially loaded on every 40^{th} row so that an even and orderly seed grid with row and column spacings of 1000m is generated.

Autotracker Tool

Traptester's autotracker tool was used to automatically populate horizon data laterally through the seismic volume. Autotracker data begins at seed horizons and proceeds along events of similar amplitude according to user-defined parameters. The autotracker was used to accelerate the horizon mapping process by filling gaps between seed where the reflectors were continuous.

The autotracker parameters were programmed with the aim of limiting automatic data population in areas with low quality or discontinuous reflectors. The autotracker was programmed to terminate at faults.

The final parameters used to track each horizon are as follows:

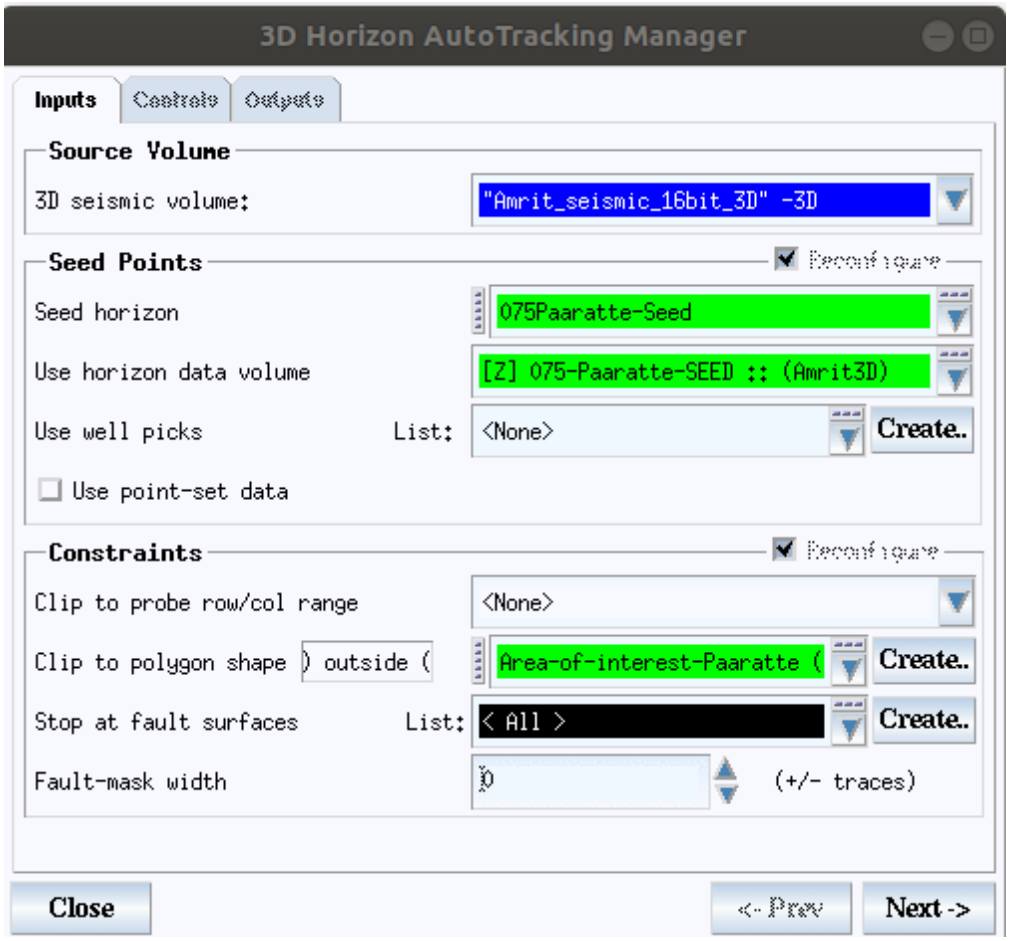

The auto-tracker stops at fault surfaces, so seed points need to be present within each fault block for the auto-tracker to populate the region with data.

The seed volume is the data created by tracing of horizon data on in-lines and cross-lines. Care should be taken not to overwrite this data. The aim of this procedure is to write a new volume of autotracked data for the same horizon, but for a separate volume.

The parameters used for the autotracker are explained on the following page.

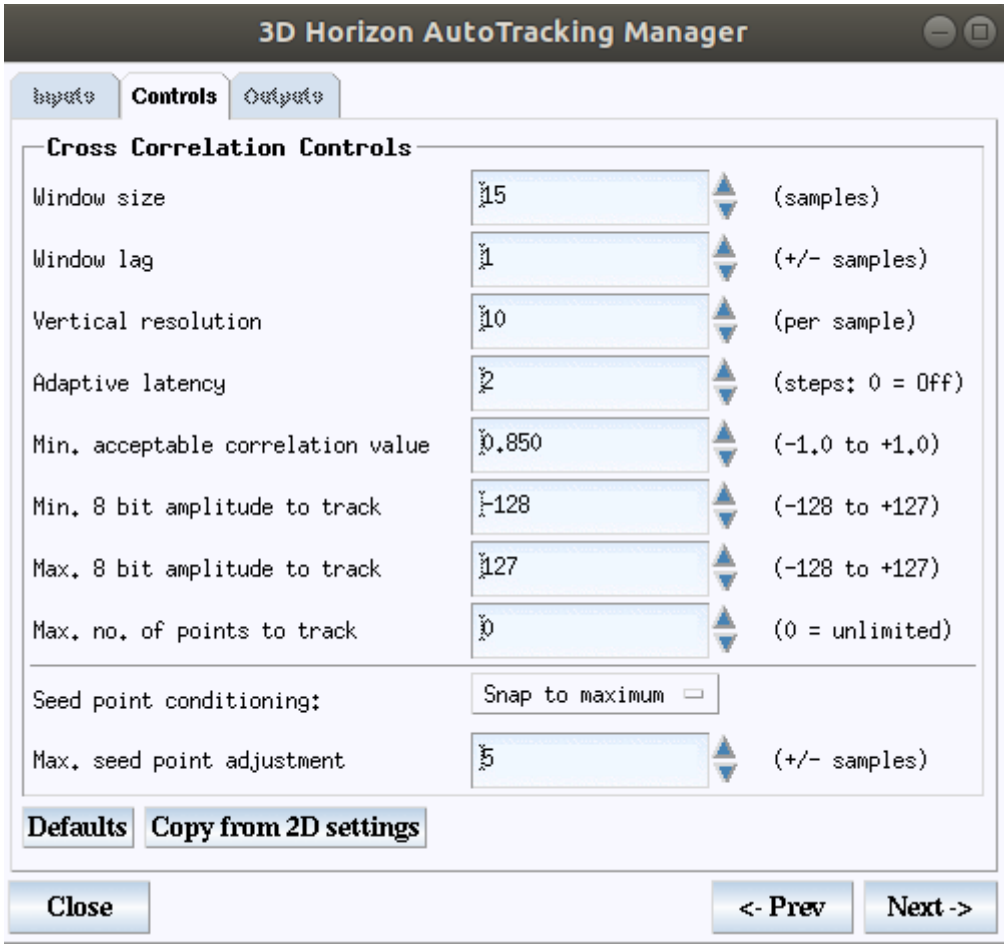

Settings used for cross correlation control for final seismic horizons, see below for parameter descriptions.

The cross-correlation controls define how the autotracker propagates from the seed pints through the tracking medium.

The window size is the vertical height of the window that the autotracker uses to cross correlate. In this case set to 15 samples to restrict the autotracker window to the waveform being tracked.

The window lag is the maximum height (in samples) that the comparison trace may be shifted correlate with the previous trace. A value of 1 is used for all horizons in this study.

Vertical Resolution allows the option to resample the trace to create a smoother output horizon at the expense of computation time. For the final horizons, a vertical resolution of 10 is used to guarantee high resolution outputs.

Adaptive Latency determines the number of previous traces to be referenced by the autotracker during cross-correlation with the next trace to be tracked. This allows the autotracker to respond better to lateral variations in the waveform shape.

Minimum acceptable correlation value limits the autotracker from propagating through traces with correlation values less than the user defined value. The range of values is -1 (poor match) to +1 (identical traces). The limit can be adjusted to exclude badly matching traces from the tracking, though final values used for horizons in this study were .85.

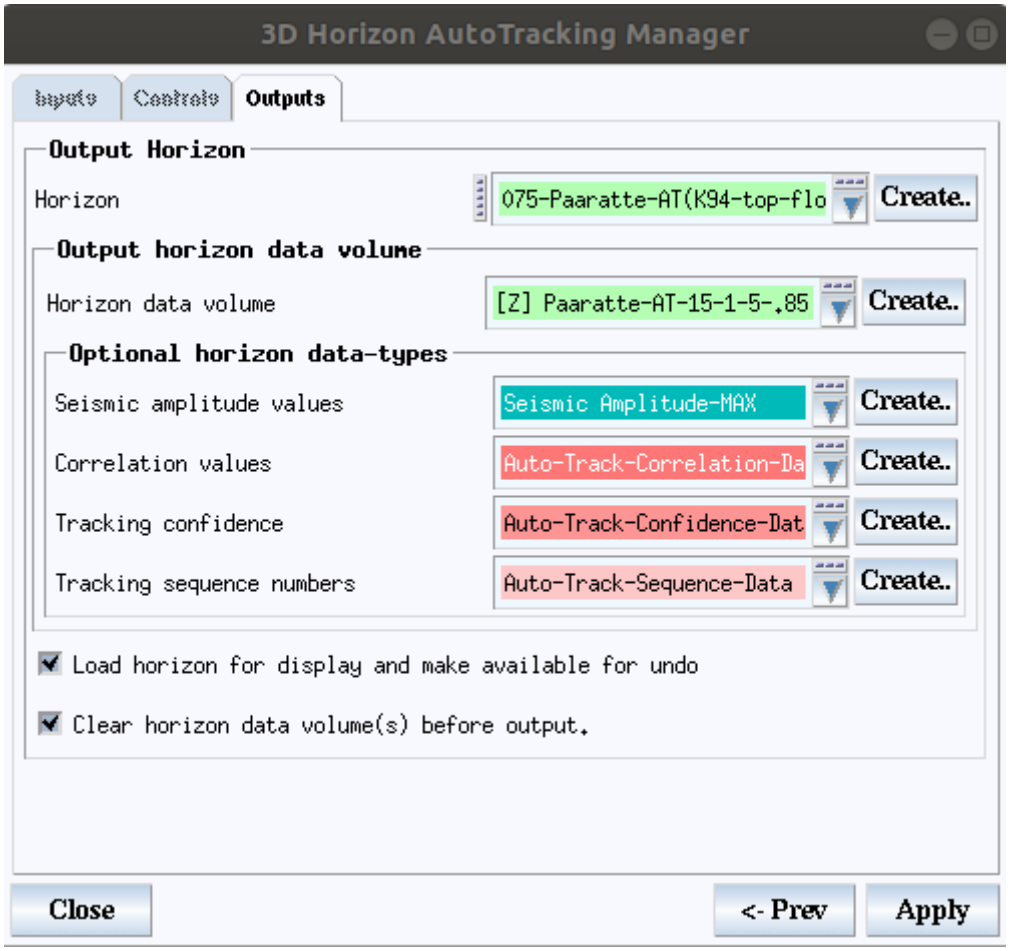

The autotrack data is written to a new volume and the outputs written to that volume are selected below under "optional horizon data-types".

The min and or max 8-bit value to track is left at full range of -128 to 127.

The maximum number of points to track was set to 0 so as not to limit the autotracker area.

Seed point conditioning was set to maximum, in this sample most horizons were picked on peaks, in this seismic volume peaks represent the boundary property of a transition from hard into soft lithology.

The maximum seed point adjustment was left at the default of +/- 5 samples.

The auto tracker data output was directed to a new data volume in a separate newly created horizon. The Seed horizon and the auto-track horizon can then be loaded separately into the volume editor.

Manual editing of horizon auto track data near faults is be necessary since data quality tends to deteriorate with proximity to faults.

Raw auto track data was manually deleted in areas where deterioration of the signal quality caused the auto tracker to leap above or below the desired reflector.

Horizon flattening

Horizon flattening methods were used to check internal consistency of interpreted horizons. Seismic cross sections were flattened along selected horizons using a previously tracked horizons as a datum. Any sharp breaks in the seismic, including the seafloor reflector, suggests a miscorrelation is present within the flattened horizon. Horizon flattening was used as a visual aid for understanding sediment dispersal and accumulation during early stages of interpretation.

Modelling Horizon-Fault Intersection Polygons

A key feature of a geological faulted framework model is that the horizons and faults fit together in an air-tight fashion. Where horizons intersect with fault planes forms two lines across the surface of the fault, one at the footwall horizon intersection and one at the hangingwall horizon intersection. These horizon fault intersection polygons are often referred to simply as ‘polygons’. The accuracy of horizon/fault intersections is key to creating a framework that is air-tight. The importance of accurate fault intersection polygons is also important for fault statistics modelling, because these intersection polygons will be used to compute fault surface attributes such as throw and other attributes used in this study. Fault horizon intersection polygons are also used to compute shear strain, and longitudinal strain; two important attributes that can be used to check the quality of faults/accuracy of an interpretation.

A function within Traptester automatically creates intersection polygons by projecting raw autotrack data onto the fault surface. These polygons can be subsequently edited on a per fault basis. To accelerate workflow and accuracy, seismic slices from 50m away from the footwalls and hangingwalls of faults and projected onto the fault surfaces as display attributes so that reflectors can be recognised used to ensure intersection polygon locations are accurately located on the fault surfaces.

Trim Distance and Patch width

Trim distance and patch width were set to 60m and 40m respectively, in project parameters. These tools help circumvent the issue of autotrack noise near faults being translated during intersection polygon modelling. The trim function excludes auto-track data from a specified distance to the fault surface from use in polygon modelling. The patch function is a surface interpolated across horizon auto-track data that is used to project fault horizon intersection polygons onto fault surfaces. Wider patches sample more horizon autotrack data away from the fault, resulting in smoother automatic modelling of intersection polygons.

Time to depth conversion of the 3-D volume.

Checkshot data for the Amrit-1 well and Hill-1 well involved in the conversion of data from the time domain (two-way travel time) to the depth domain (metres) is shown below.

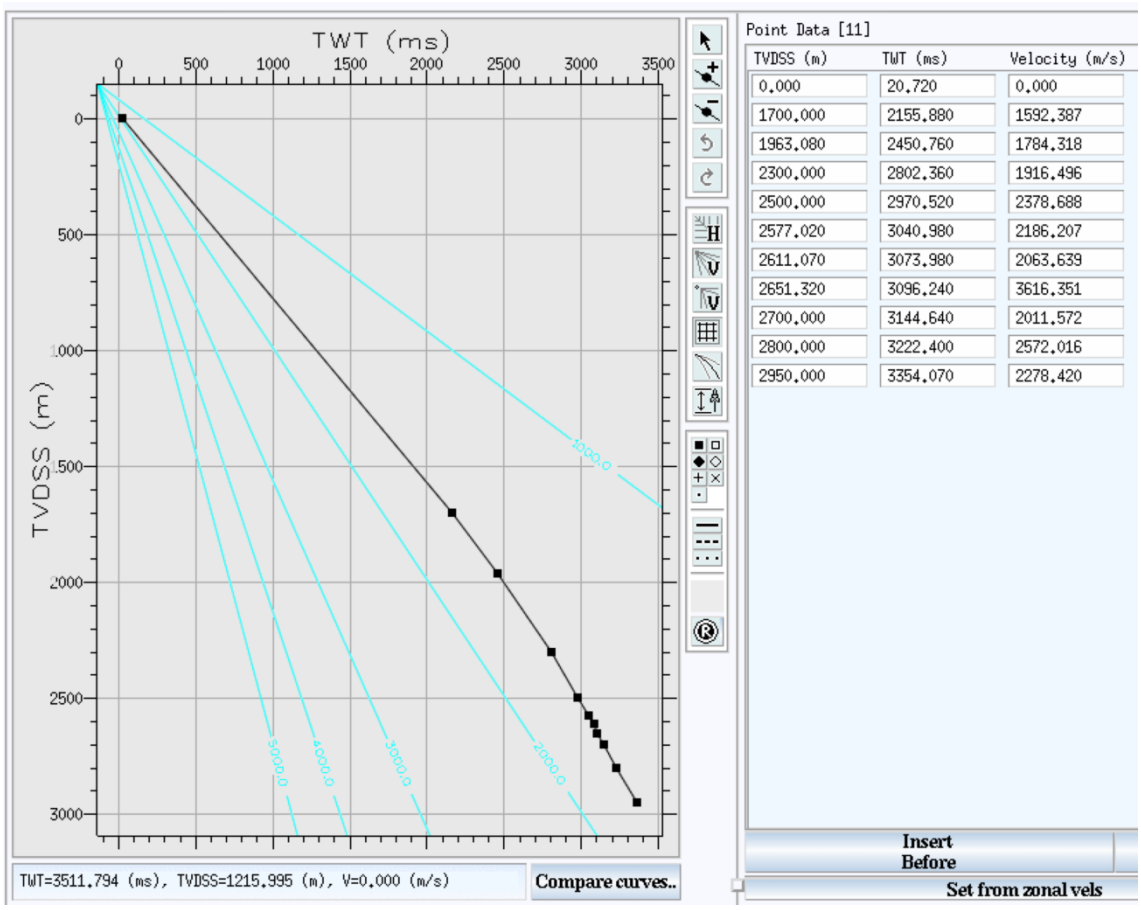

Amrit-1 well time-depth curve and check shot data.

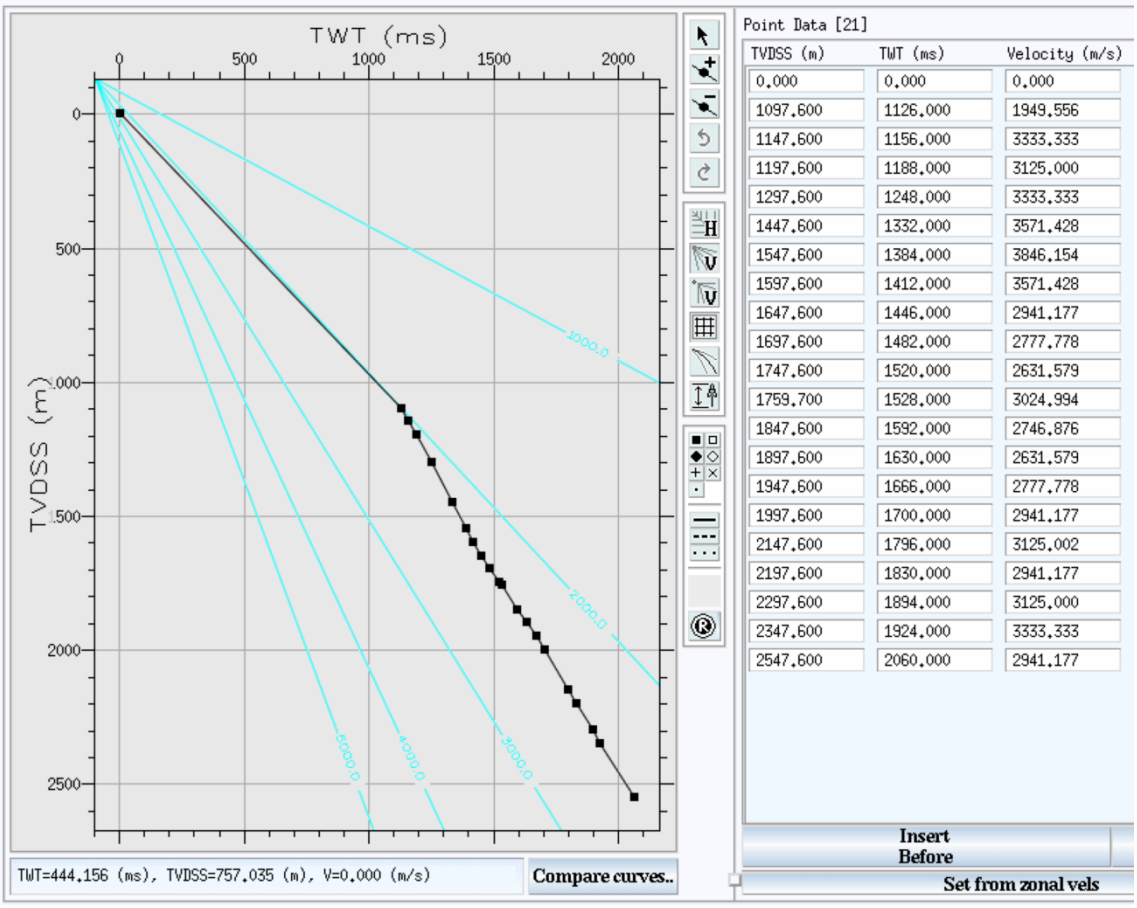

Hill-1 well time-depth curve and check shot data.

The time-depth conversion was performed using a velocity model provided by cooper energy. The velocity model used was an interval velocity model, a 3-D volume with velocity values of strata between previously selected horizons. The procedure to convert from time to depth was performed in Traptester using project > convert time to depth > selecting the file path of the velocity segy volume, selecting the interval velocity option, selecting a name for the new project in depth, and applying.